Pergamon

J. Quant. Spectrosc. Radiat. Transfer Vol. 56, No. 5, pp. 673–702, 1996

PII: S0022-4073(96)00117-3
0022-4073/96 $15.00 + 0.00

DIFFUSE AND COHERENT BACKSCATTERING BY DISCRETE RANDOM MEDIA—I. RADAR REFLECTIVITY, POLARIZATION RATIOS, AND ENHANCEMENT FACTORS FOR A HALF-SPACE OF POLYDISPERSE, NONABSORBING AND ABSORBING SPHERICAL PARTICLES

MICHAEL I. MISHCHENKO

NASA Goddard Institute for Space Studies and Institute of Terrestrial and Planetary Atmospheres/State University of New York at Stony Brook, 2880 Broadway, New York, NY 10025, U.S.A.

(Received 3 April 1996)

Abstract—It has been demonstrated recently that diffuse, incoherent multiple scattering of electromagnetic waves by media composed of randomly positioned, discrete scattering particles is always accompanied by coherent backscattering and may explain intriguing opposition phenomena observed for some solar system bodies, in particular peculiar characteristics of radar returns from icy satellite surfaces. In this paper, we study theoretically photometric and polarization characteristics of diffuse and coherent backscattering by discrete random media. The cyclical component of the Stokes reflection matrix at exactly the backscattering direction is expressed in terms of the ladder component, and the ladder component is accurately computed by numerically solving the vector radiative transfer equation. We give formulas expressing the radar reflectivity, radar linear and circular polarization ratios, and backscattering enhancement factors in the elements of the Stokes reflection matrix and describe in detail the computational technique used. Assuming that the scattering medium is homogeneous and semi-infinite and that scattering particles are polydisperse spheres, we report the results of a comprehensive theoretical survey of the dependence of the photometric and polarization characteristics of the radar return on the illumination zenith angle and on the particle effective size parameter and real and imaginary parts of the refractive index. Copyright © 1996 Elsevier Science Ltd

1. INTRODUCTION

It has been realized recently that diffuse, incoherent multiple scattering of electromagnetic waves by media composed of randomly positioned, discrete scattering particles is always accompanied by a phenomenon called coherent backscattering (or weak localization). This phenomenon has been intensively investigated during the last decade both experimentally and theoretically.[1–3] Furthermore, by comparing observational data with theoretical computations, it has been shown that coherent backscattering of sunlight by regolithic grains can be responsible for two spectacular natural phenomena exhibited by Saturn's rings and some atmosphereless solar system bodies, namely, the photometric[4,5] and polarization[6] opposition effects (see also Refs. 7–11). Also, it has been suggested that diffuse and coherent backscattering of electromagnetic waves might explain unusual radar returns for icy outer planet satellites, polar caps on Mars and Mercury, and some terrestrial lava flows.[9,12–17] In this case, multiple scattering may be caused by discrete scatterers in a relatively transparent matrix, e.g., by particulate rock and/or ice surfaces in air or rocks imbedded in ice.

The physics of coherent backscattering is basically well understood[1–3] and assumes that multiply scattered radiation reflected by discrete disordered media is composed of two parts. The first part is the incoherent, diffuse radiation coming from the first-order-scattering contribution and the sum of so-called ladder terms of the Bethe–Salpeter equation.[18] The second part is the coherent backscattering peak, which is produced by interference of conjugate pairs of waves scattered

along the following paths: (1) [source of light] → [particle 1] → [particle 2] → . . . → [particle $N-1$] → [particle N] → [detector] and (2) [source of light] → [particle N] → [particle $N-1$] → . . . → [particle 2] → [particle 1] → [detector] (Fig. 1). At exactly the backscattering direction (viewing direction is exactly opposite to the illumination direction so that the phase angle α is equal to zero), the interference of the two waves is always constructive regardless of what particular configuration of particles is involved and causes a distinct backscattering enhancement of the reflected intensity. The coherent part of the reflected radiation comes from the sum of so-called cyclical terms of the Bethe–Salpeter equation.[18]

Owing to its fundamental interference nature, coherent backscattering is a universal physical phenomenon, accompanies any multiple-scattering process, and occurs for particles of any size, shape, and refractive index. In other words, it is not necessary to require that scattering particles be wavelength-sized, as it is sometimes done in applied literature. The angular width of the backscattering intensity peak can be very small for particles much smaller or much larger than the wavelength of the incident radiation,[5,6] thus often making the peak unobservable in passive remote sensing observations. However, coherent backscattering almost always affects active remote sensing measurements with monostatic lidars and radars, e.g., radar observations of planets.[17]

Because of complicated multiple-scattering processes involved, accurate computations of coherent backscattering must be based on elaborated theoretical techniques. The conventional theoretical tool for computing coherent backscattering by discrete random media has been the diffusion approximation.[1–3,19,20] However, although the diffusion approximation rather accurately predicts the angular profile of the backscattering intensity peak, it ignores the first-order-scattering contribution to the reflected light and, thus, cannot be used to compute the amplitude of the peak, i.e., the ratio of the intensity at the center of the peak to the incoherent background intensity. Moreover, in some cases the main physical characteristics of a particulate medium (e.g., particle size, shape, and refractive index) are not explicit model parameters,[13] thus making difficult, if at all possible, comparisons of model computations with results of controlled laboratory experiments. An additional complexifying factor is that accurate computation of the amplitude and polarization state of the backscattering peak must explicitly take into account the vector nature of light since polarization effects have been shown to be extremely important in coherent backscattering.[3,6,21–25]

Reflection of polarized light by a discrete random medium can be described by a 4×4 Stokes reflection matrix consisting of the first-order-scattering, ladder, and cyclical components.[3] In a recent publication,[24] the author has used the reciprocity principle[26] to derive a rigorous relationship between the cyclical and ladder components of the reflection matrix at exactly the backscattering

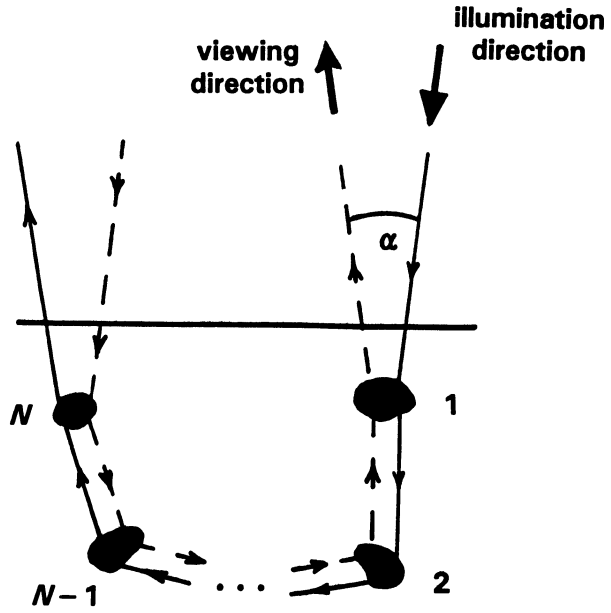

Fig. 1. Schematic explanation of the interference nature of coherent backscattering.

direction. This relationship represents one of a very few rigorous results of the vector theory of coherent backscattering (see, also, Ref. 25) and is very useful in practice owing to the following three factors. First, in the derivation of this relationship, the vector nature of light has been fully taken into account. Second, it is well known[27,28] that the first-order-scattering and ladder components of the reflection matrix can be rigorously computed by solving the vector radiative transfer equation[18,29,30] with one of the well established numerical techniques.[31–36] Therefore, this relationship can be used to compute the cyclical component of the reflection matrix at the center of the backscattering peak and, thus, the amplitude of the peak. Third, particle size, shape, and refractive index are explicit model parameters, thus facilitating comparisons of theoretical computations with controlled laboratory experiments. The only approximation involved in this approach is the assumption that particles forming the discrete random medium are independent scatterers. For densely packed particles, this assumption may not be quite true. Unfortunately, rigorous theoretical computations of multiple light scattering by closely spaced wavelength-sized particles based on directly solving Maxwell's equations are currently possible only for simplest scattering configurations composed of a few components (see, e.g., Ref. 37, which shows that polydisperse, randomly oriented bispheres with widely separated wavelength-sized components exhibit coherent backscattering). Therefore, the assumption of independent scattering has to be made if optically thick scattering media composed of a very large number of particles (e.g., planetary regoliths) are to be considered. It should be noted, however, that, as calculations reported in Ref. 38 suggest, the primary effect of spatial correlation among densely packed particles may be to modify the particles' forward-scattering behavior, thus indicating that radiative transfer calculations for the backscattering direction can be reasonably accurate even if particles are densely packed. Apparently, this explains the excellent quantitative agreement between radiative transfer computations[39] and controlled laboratory measurements of coherent backscattering for dense suspensions of latex microspheres in water.[21,40]

The approach developed in Ref. 24 was later used in Ref. 12 for computing the photometric and polarization characteristics of coherent backscattering for semi-infinite media composed of polydisperse spherical particles. Unfortunately, the low speed of the computer used (a 286-based PC) restricted the scope of that study to only eight scattering models. A much more powerful computer available to the author now (an IBM RISC model 37T workstation) makes possible a comprehensive theoretical survey of the dependence of diffuse and coherent backscattering characteristics on such basic physical parameters of the scattering medium as particle size parameter, refractive index, and shape. In this first paper of a series, we focus on the quantities that describe the photometric and polarimetric characteristics of a radar return, i.e., on the radar backscattering coefficient and radar polarization ratios.[17,18] For simplicity, we assume that the scattering medium is homogeneous and semi-infinite and is composed of polydisperse spherical particles. In the following section we introduce basic definitions relevant to the vector theory of diffuse and coherent backscattering and describe in detail the theoretical technique for computing the ladder and cyclical components of the Stokes reflection matrix for a discrete random medium. In Sec. 3, we introduce radar definitions and derive formulas expressing the radar backscattering coefficient, radar linear and circular polarization ratios, and backscattering enhancement factors in the elements of the Stokes reflection matrix. Section 4 reports results of computer calculations for a wide range of particle size parameters and real and imaginary parts of the refractive index and discusses the effect of these parameters on the characteristics of the radar return. The results of the paper are summarized in the concluding section.

2. POLARIMETRIC DEFINITIONS AND COMPUTATIONAL METHOD

We assume that the scattering medium is homogeneous and optically semi-infinite, has a macroscopically flat boundary, and is composed of randomly positioned discrete particles. Also, we assume that the medium is macroscopically isotropic and symmetric, which means that the particles comprising the medium are randomly oriented and each particle has a plane of symmetry and/or particles and their mirror counterparts occur in equal numbers. To describe the geometry of multiple light scattering, we use a right-handed Cartesian coordinate system with the z-axis directed along the outward normal to the boundary, as shown in Fig. 2. The direction of light

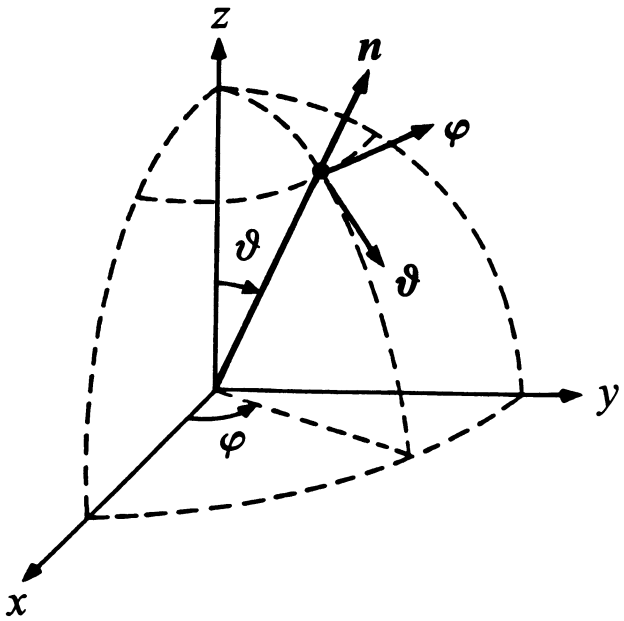

Fig. 2. On the geometry of multiple light scattering.

propagation is specified by the unit vector $\mathbf{n}$ or, equivalently, by the couple (u, φ), where $u = -\cos\vartheta$, ϑ is the zenith angle measured from the positive z-axis, and φ is the azimuth angle measured from the positive x-axis in the clockwise direction when looking upwards. Note that $u < 0$ for upwelling radiation and $u > 0$ for downwelling radiation. Also, we define $\mu = |u|$. To describe the intensity and state of polarization of a beam of light, we use the local right-handed orthonormal system formed by the unit vectors $\mathbf{n}$, $\boldsymbol{\vartheta}$, and $\boldsymbol{\varphi}$ given by

$$\boldsymbol{\varphi} = \frac{\mathbf{z} \times \mathbf{n}}{|\mathbf{z} \times \mathbf{n}|} \tag{1}$$

and

$$\boldsymbol{\vartheta} = \boldsymbol{\varphi} \times \mathbf{n}, \tag{2}$$

where $\mathbf{z}$ is a unit vector in the positive z-direction. In other words, the unit vector $\boldsymbol{\vartheta}$ lies in the meridian plane of the beam (the plane through the beam and the local z-axis), while the unit vector $\boldsymbol{\varphi}$ is perpendicular to this plane. Note that

$$\mathbf{n} = \boldsymbol{\vartheta} \times \boldsymbol{\varphi}. \tag{3}$$

Thus, we use in this paper the so-called forward scattering alignment convention (or wave coordinates) rather than the backscatter alignment convention (or antenna coordinates).[41,42]

Following Refs. 31 and 43, we define, up to a multiplicative constant, the Stokes parameters I, Q, U, and V of a quasi-monochromatic beam of radiation as

$$I = \langle E_\vartheta E_\vartheta^* + E_\varphi E_\varphi^* \rangle, \tag{4}$$

$$Q = \langle E_\vartheta E_\vartheta^* - E_\varphi E_\varphi^* \rangle, \tag{5}$$

$$U = -\langle E_\vartheta E_\varphi^* + E_\varphi E_\vartheta^* \rangle, \tag{6}$$

$$V = i\langle E_\varphi E_\vartheta^* - E_\varphi E_\varphi^* \rangle, \tag{7}$$

where E_ϑ and E_φ are the ϑ- and φ-components of the electric field, respectively, the asterisk denotes the complex-conjugate value, and angular brackets denote time averaging. Note that sometimes the ϑ- and φ-components of the electric field are called the vertical and horizontal components and denoted as E_v and E_h, respectively.[18] The first Stokes parameter, I, is the common intensity,

while the other three Stokes parameters specify the state of polarization of the beam of light. The Stokes vector is defined as a four-component column having the Stokes parameters as its components:

$$\mathbf{I} = \begin{bmatrix} I \\ Q \\ U \\ V \end{bmatrix}. \tag{8}$$

Let the medium be illuminated by a parallel beam of quasi-monochromatic radiation incident in the direction (μ_0, φ_0) and characterized by the Stokes vector $\mathbf{I}_0$ so that I_0 is the incident energy flux per unit area perpendicular to the beam. The Stokes vector of radiation reflected by the medium in the direction $(-\mu, \varphi)$ is given by

$$\mathbf{I}(-\mu, \varphi) = \frac{1}{\pi}\mu_0 \mathbf{S}(\mu, \mu_0, \varphi - \varphi_0)\mathbf{I}_0, \tag{9}$$

where $\mathbf{S}(\mu, \mu_0, \varphi - \varphi_0)$ is the Stokes reflection matrix of dimension (4×4). Note that the reflection matrix relates the Stokes parameters of the incident and scattered beams specified with respect to their local meridian planes rather than with respect to the scattering plane (viz., the plane through the incident and reflected beams). Since we assume that the scattering medium is macroscopically isotropic and symmetric, the reflection matrix depends on the difference between the azimuth angles of the incident and reflected beams rather than on each of the azimuth angles separately.[31]

The reflection matrix can be decomposed as[3]

$$\mathbf{S}(\mu, \mu_0, \varphi - \varphi_0) = \mathbf{S}^{1}(\mu, \mu_0, \varphi - \varphi_0) + \mathbf{S}^{L}(\mu, \mu_0, \varphi - \varphi_0) + \mathbf{S}^{C}(\mu, \mu_0, \varphi - \varphi_0), \tag{10}$$

where 1 denotes the first-order-scattering component, L denotes the ladder component, and C denotes the cyclical component. The first-order-scattering and ladder components of the reflection matrix are rather slowly varying functions of the reflection direction, and their sum describes the diffuse, incoherent background of the reflected radiation. The cyclical component of the reflection matrix $\mathbf{S}^{C}(\mu, \mu_0, \varphi - \varphi_0)$ describes the effect of coherent backscattering, which is superposed on the diffuse background. Unlike $\mathbf{S}^{1}(\mu, \mu_0, \varphi - \varphi_0)$ and $\mathbf{S}^{L}(\mu, \mu_0, \varphi - \varphi_0)$, $\mathbf{S}^{C}(\mu, \mu_0, \varphi - \varphi_0)$ deviates from zero only in the nearest vicinity of the backscattering direction given by $(-\mu, \varphi) = (-\mu_0, \varphi_0 + \pi)$ and is zero outside the coherent backscattering peak. Both $\mathbf{S}^{1}(\mu, \mu_0, \varphi - \varphi_0)$ and $\mathbf{S}^{L}(\mu, \mu_0, \varphi - \varphi_0)$ can be found by solving numerically the vector radiative transfer equation (see below). The computation of the cyclical component $\mathbf{S}^{C}(\mu, \mu_0, \varphi - \varphi_0)$ for any μ, μ_0, and $\varphi - \varphi_0$ is a much more complicated problem which has been rigorously solved only for the case of Rayleigh scattering (i.e., for particles much smaller than the wavelength of the incident radiation)[25] and still awaits a general solution for particles of arbitrary size, shape, and refractive index. However, the rigorous relationship derived in Ref. 24 enables one to use the precomputed ladder component for calculating the cyclical component at exactly the backscattering direction, i.e., the matrix $\mathbf{S}^{C}(\mu_0, \mu_0, \pi)$. Specifically,

$$\mathbf{S}^{C}(\mu_0, \mu_0, \pi) = \begin{bmatrix} S_{11}^{C}(\mu_0, \mu_0, \pi) & S_{12}^{L}(\mu_0, \mu_0, \pi) & 0 & 0 \\ S_{12}^{L}(\mu_0, \mu_0, \pi) & S_{22}^{C}(\mu_0, \mu_0, \pi) & 0 & 0 \\ 0 & 0 & S_{33}^{C}(\mu_0, \mu_0, \pi) & S_{34}^{L}(\mu_0, \mu_0, \pi) \\ 0 & 0 & -S_{34}^{L}(\mu_0, \mu_0, \pi) & S_{44}^{C}(\mu_0, \mu_0, \pi) \end{bmatrix}, \tag{11}$$

where

$$S_{11}^{C}(\mu_0, \mu_0, \pi) = \tfrac{1}{2}[S_{11}^{L}(\mu_0, \mu_0, \pi) + S_{22}^{L}(\mu_0, \mu_0, \pi) - S_{33}^{L}(\mu_0, \mu_0, \pi) + S_{44}^{L}(\mu_0, \mu_0, \pi)], \tag{12}$$

$$S_{22}^{C}(\mu_0, \mu_0, \pi) = \tfrac{1}{2}[S_{11}^{L}(\mu_0, \mu_0, \pi) + S_{22}^{L}(\mu_0, \mu_0, \pi) + S_{33}^{L}(\mu_0, \mu_0, \pi) - S_{44}^{L}(\mu_0, \mu_0, \pi)], \tag{13}$$

$$S_{33}^{C}(\mu_0, \mu_0, \pi) = \tfrac{1}{2}[-S_{11}^{L}(\mu_0, \mu_0, \pi) + S_{22}^{L}(\mu_0, \mu_0, \pi) + S_{33}^{L}(\mu_0, \mu_0, \pi) + S_{44}^{L}(\mu_0, \mu_0, \pi)], \tag{14}$$

$$S_{44}^{C}(\mu_0, \mu_0, \pi) = \tfrac{1}{2}[S_{11}^{L}(\mu_0, \mu_0, \pi) - S_{22}^{L}(\mu_0, \mu_0, \pi) + S_{33}^{L}(\mu_0, \mu_0, \pi) + S_{44}^{L}(\mu_0, \mu_0, \pi)]. \tag{15}$$

Thus, although the complete computation of the angular profile of the coherent backscattering peak is still impossible, the combined use of the vector radiative transfer theory and Eqs. (10)–(15) provides the full specification of the reflected radiation outside the peak [Eq. (10) with $S^{C}(\mu, \mu_0, \varphi - \varphi_0) = 0$] and at exactly the center of the backscattering peak. Note that for a macroscopically isotropic and symmetric medium, the first-order-scattering and ladder components at exactly the backscattering direction have simple diagonal and block-diagonal structures, respectively [see Eqs. (18), (32), (36), and (42) below]:

$$\mathbf{S}^{1}(\mu_0, \mu_0, \pi) = \mathrm{diag}[S_{11}^{1}(\mu_0, \mu_0, \pi); S_{22}^{1}(\mu_0, \mu_0, \pi); S_{33}^{1}(\mu_0, \mu_0, \pi); S_{44}^{1}(\mu_0, \mu_0, \pi)], \tag{16}$$

$$\mathbf{S}^{L}(\mu_0, \mu_0, \pi) = \begin{bmatrix} S_{11}^{L}(\mu_0, \mu_0, \pi) & S_{12}^{L}(\mu_0, \mu_0, \pi) & 0 & 0 \\ S_{12}^{L}(\mu_0, \mu_0, \pi) & S_{22}^{L}(\mu_0, \mu_0, \pi) & 0 & 0 \\ 0 & 0 & S_{33}^{L}(\mu_0, \mu_0, \pi) & S_{34}^{L}(\mu_0, \mu_0, \pi) \\ 0 & 0 & -S_{34}^{L}(\mu_0, \mu_0, \pi) & S_{44}^{L}(\mu_0, \mu_0, \pi) \end{bmatrix}. \tag{17}$$

As was mentioned above, the sum of the first-order-scattering and ladder components of the reflection matrix, $\mathbf{R}(\mu, \mu_0, \varphi - \varphi_0) = \mathbf{S}^{1}(\mu, \mu_0, \varphi - \varphi_0) + \mathbf{S}^{L}(\mu, \mu_0, \varphi - \varphi_0)$, describes the reflected radiation outside the backscattering peak (i.e., the diffuse background) and can be computed by solving numerically the vector radiative transfer equation. de Haan et al[34] have shown that a convenient and efficient way of treating the azimuthal dependence of the diffuse reflection matrix $\mathbf{R}(\mu, \mu_0, \varphi - \varphi_0)$ is to expand it in a special Fourier series

$$\begin{aligned} \mathbf{R}(\mu, \mu_0, \varphi - \varphi_0) = \frac{1}{4} \sum_{m=0}^{M} (2 - \delta_{m0}) \{ & [(\mathbf{E} + \mathbf{D})\mathbf{R}^{m}(\mu, \mu_0)(\mathbf{E} + \mathbf{D}) \\ & + (\mathbf{E} - \mathbf{D})\mathbf{R}^{m}(\mu, \mu_0)(\mathbf{E} - \mathbf{D})] \cos m(\varphi - \varphi_0) + [(\mathbf{E} - \mathbf{D})\mathbf{R}^{m}(\mu, \mu_0)(\mathbf{E} + \mathbf{D}) \\ & - (\mathbf{E} + \mathbf{D})\mathbf{R}^{m}(\mu, \mu_0)(\mathbf{E} - \mathbf{D})] \sin m(\varphi - \varphi_0) \}, \end{aligned} \tag{18}$$

where

$$\mathbf{E} = \mathrm{diag}[1, 1, 1, 1], \tag{19}$$

$$\mathbf{D} = \mathrm{diag}[1, 1, -1, -1], \tag{20}$$

and the upper summation limit M depends on the desired accuracy of computations. We compute the Fourier components of the diffuse reflection matrix $\mathbf{R}^{m}(\mu, \mu_0)$ for a semi-infinite homogeneous medium by solving numerically the Ambartsumian's nonlinear integral equation[29,44]

$$\begin{aligned} (\mu + \mu_0)\mathbf{R}^{m}(\mu, \mu_0) = & \frac{w}{4} \mathbf{Z}^{m}(-\mu, \mu_0) \\ & + \frac{w}{2} \mu \int_0^1 d\mu' \mathbf{R}^{m}(\mu, \mu') \mathbf{Z}^{m}(\mu', \mu_0) + \frac{w}{2} \mu_0 \int_0^1 d\mu' \mathbf{Z}^{m}(-\mu, -\mu') \mathbf{R}^{m}(\mu', \mu_0) \\ & + w\mu\mu_0 \int_0^1 \int_0^1 d\mu' d\mu'' \mathbf{R}^{m}(\mu, \mu') \mathbf{Z}^{m}(\mu', -\mu'') \mathbf{R}^{m}(\mu'', \mu_0). \end{aligned} \tag{21}$$

This equation is a consequence of the invariance of the matrix $\mathbf{R}(\mu, \mu_0, \varphi - \varphi_0)$ when an infinitesimally thin layer is added on top of a semi-infinite medium and can be derived from Eq. (3.51) of Ref. 31 by zeroing its left-hand side. In Eq. (21), w is the albedo for single scattering and (4×4) matrices $\mathbf{Z}^{m}(u, u')$ are Fourier components of the phase matrix $\mathbf{Z}(u, u', \varphi - \varphi')$. The phase matrix describes the angular distribution and the change of the polarization state of light singly scattered by a small-volume element and relates the Stokes parameters of the incident and scattered beams specified with respect to their own meridian planes.[18,43]

The Fourier components of the phase matrix are given by[34]

$$\mathbf{Z}^m(u, u') = (-1)^m \sum_{s=m}^{s_{\max}} \mathbf{P}_m^s(u)\mathbf{S}^s\mathbf{P}_m^s(u'), \quad u, u' \in [-1, 1], \tag{22}$$

where the matrices $\mathbf{P}_m^s(u)$ are defined as

$$\mathbf{P}_m^s(u) = \begin{bmatrix} P_{m0}^s(u) & 0 & 0 & 0 \\ 0 & P_{m+}^s(u) & P_{m-}^s(u) & 0 \\ 0 & P_{m-}^s(u) & P_{m+}^s(u) & 0 \\ 0 & 0 & 0 & P_{m0}^s(u) \end{bmatrix} \tag{23}$$

and

$$P_{m\pm}^s(u) = \tfrac{1}{2}[P_{m,-2}^s(u) \pm P_{m2}^s(u)], \tag{24}$$

and $P_{mn}^s(u)$ are generalized spherical functions.[43] The matrices $\mathbf{S}^s$ have the form

$$\mathbf{S}^s = \begin{bmatrix} a_1^s & b_1^s & 0 & 0 \\ b_1^s & a_2^s & 0 & 0 \\ 0 & 0 & a_3^s & b_2^s \\ 0 & 0 & -b_2^s & a_4^s \end{bmatrix}. \tag{25}$$

The elements of these matrices are the coefficients that appear in the following expansions:

$$F_{11}(\Theta) = \sum_{s=0}^{s_{\max}} a_1^s P_{00}^s(\cos\Theta), \tag{26}$$

$$F_{22}(\Theta) + F_{33}(\Theta) = \sum_{s=2}^{s_{\max}} (a_2^s + a_3^s) P_{22}^s(\cos\Theta), \tag{27}$$

$$F_{22}(\Theta) - F_{33}(\Theta) = \sum_{s=2}^{s_{\max}} (a_2^s - a_3^s) P_{2,-2}^s(\cos\Theta), \tag{28}$$

$$F_{44}(\Theta) = \sum_{s=0}^{s_{\max}} a_4^s P_{00}^s(\cos\Theta), \tag{29}$$

$$F_{12}(\Theta) = \sum_{s=2}^{s_{\max}} b_1^s P_{02}^s(\cos\Theta), \tag{30}$$

$$F_{34}(\Theta) = \sum_{s=2}^{s_{\max}} b_2^s P_{02}^s(\cos\Theta), \tag{31}$$

where Θ is the scattering angle (angle between the incident and scattered beams) and $F_{ij}(\Theta)$ are elements of the scattering matrix:

$$\mathbf{F}(\Theta) = \begin{bmatrix} F_{11}(\Theta) & F_{12}(\Theta) & 0 & 0 \\ F_{12}(\Theta) & F_{22}(\Theta) & 0 & 0 \\ 0 & 0 & F_{33}(\Theta) & F_{34}(\Theta) \\ 0 & 0 & -F_{34}(\Theta) & F_{44}(\Theta) \end{bmatrix}. \tag{32}$$

The (1,1) element of the scattering matrix is called the scattering phase function and is normalized to unity:

$$\tfrac{1}{2}\int_0^{\pi} \mathrm{d}\Theta \sin\Theta F_{11}(\Theta) = 1. \tag{33}$$

In contrast to the phase matrix $\mathbf{Z}(u, u', \varphi - \varphi')$ which is referenced to the local meridian planes of the incident and scattered beams, the scattering matrix relates the Stokes parameters of the

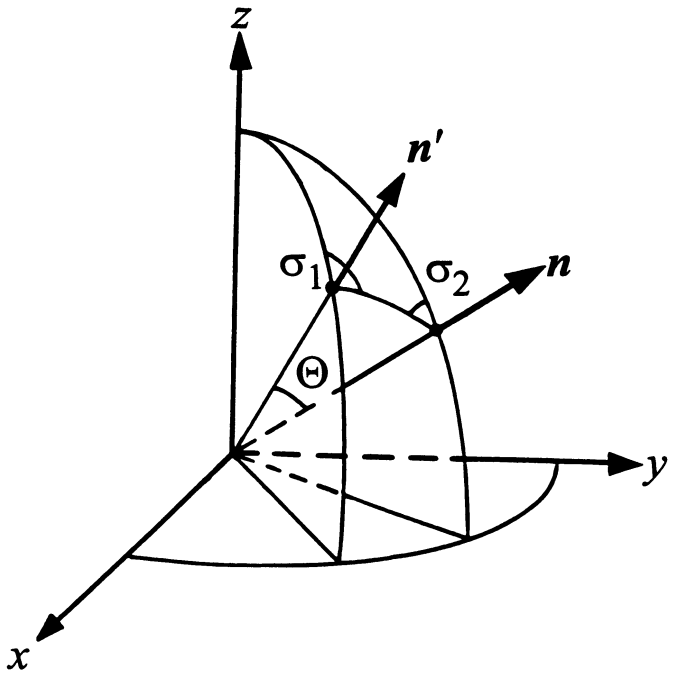

Fig. 3. On the relationship between the scattering and phase matrices.

incident and scattered beams specified with respect to the scattering plane, i.e., the plane through the two beams. The relationship between the two matrices is given by[43]

$$\mathbf{Z}(\mathbf{n}, \mathbf{n}') \equiv \mathbf{Z}(u, u', \varphi - \varphi') = \mathbf{L}(\sigma_2)\mathbf{F}(\Theta)\mathbf{L}(\sigma_1), \tag{34}$$

where the (4 × 4) rotation matrix is defined as

$$\mathbf{L}(\sigma) = \begin{bmatrix} 1 & 0 & 0 & 0 \\ 0 & \cos 2\sigma & \sin 2\sigma & 0 \\ 0 & -\sin 2\sigma & \cos 2\sigma & 0 \\ 0 & 0 & 0 & 1 \end{bmatrix}, \tag{35}$$

and the angles σ_1 and σ_2 are shown in Fig. 3. The block-diagonal form of the scattering matrix of Eq. (32) follows from the assumption that the scattering medium is macroscopically isotropic and symmetric.[45] Note that

$$F_{12}(0) = F_{12}(\pi) = F_{34}(0) = F_{34}(\pi) = 0, \tag{36}$$

$$F_{33}(0) = F_{22}(0), \quad F_{33}(\pi) = -F_{22}(\pi), \tag{37}$$

and[46]

$$F_{44}(\pi) = F_{11}(\pi) - 2F_{22}(\pi). \tag{38}$$

Furthermore, for spheres,

$$F_{22}(\Theta) \equiv F_{11}(\Theta), \tag{39}$$

$$F_{44}(\Theta) \equiv F_{33}(\Theta). \tag{40}$$

Equation (26) is the standard expansion of the phase function in Legendre polynomials.[47]

The computation of the diffuse reflection matrix $\mathbf{R}(\mu, \mu_0, \varphi - \varphi_0)$ consists of the following four major numerical steps:

(1) Calculation of the single-scattering albedo w and the expansion coefficients appearing in expansions (26)–(31) for a given particle model. Fast numerical techniques for computing

the expansion coefficients for polydisperse spherical particles based on Mie theory are discussed by de Rooij and van der Stap.[48]

(2) Computation of the Fourier components of the phase matrix via Eqs. (22)–(25). Efficient recurrence relations for computing the generalized spherical functions are given by de Haan et al.[34]

(3) Computation of the Fourier components of the matrix $\mathbf{R}(\mu, \mu_0, \varphi - \varphi_0)$ by solving numerically the Ambartsumian's nonlinear integral equation. Using a Gaussian quadrature formula for numerical evaluation of integrals in Eq. (21), we obtain a system of nonlinear algebraic equations

$$(\mu_i + \mu_j)\mathbf{R}^m(\mu_i, \mu_j) = \frac{w}{4}\mathbf{Z}^m(-\mu_i, \mu_j) + \frac{w}{2}\mu_i \sum_{k=1}^{N_G} w_k \mathbf{R}^m(\mu_i, \mu_k)\mathbf{Z}^m(\mu_k, \mu_j)$$

$$+\frac{w}{2}\mu_j \sum_{k=1}^{N_G} w_k \mathbf{Z}^m(-\mu_i, -\mu_k)\mathbf{R}^m(\mu_k, \mu_j)$$

$$+ w\mu_i\mu_j \sum_{k=1}^{N_G}\sum_{k'=1}^{N_G} w_k w_{k'} \mathbf{R}^m(\mu_i, \mu_k)\mathbf{Z}^m(\mu_k, -\mu_{k'})\mathbf{R}^m(\mu_{k'}, \mu_j), \tag{41}$$

where μ_k and w_k ($k = 1, \ldots, N_G$) are Gaussian division points and weights on the interval [0, 1], respectively. For single scattering albedos w not equal to unity, this system is solved by the method of simple iterations. For conservatively scattering particles ($w = 1$), the method of simple iterations does not provide a converged solution[49] and must be supplemented by a special procedure developed by Dlugach and Yanovitskij[50] in the scalar case (i.e., when polarization of multiply scattered light is ignored) and extended by de Rooij[32] to the vector case.

(4) Calculation of the total diffuse reflection matrix $\mathbf{R}(\mu, \mu_0, \varphi - \varphi_0)$ by evaluating the Fourier series of Eq. (18).

We use several simple numerical recipes to significantly enhance the efficiency and accuracy of the computer code. First, we ensure energy conservation by renormalizing the zeroth Fourier component of the phase matrix as suggested by Hansen.[51] Second, we employ symmetry relations for the Fourier components of the reflection matrix,[34,36] thereby saving nearly 50% of CPU time. Third, we diagonalize the matrices $\mathbf{P}_m^s(u)$ and use the supermatrix approach as described by de Haan et al.[34]

By expanding the Ambartsumian's nonlinear integral equation in a Newmann order-of-scattering series over w and taking into account Eqs. (34)–(38), it is easy to show that the first-order-scattering component of the reflection matrix at exactly the backscattering direction is given by[34]

$$\mathbf{S}^1(\mu_0, \mu_0, \pi) = \frac{w}{8\mu_0}\mathbf{Z}(-\mu_0, \mu_0, \pi)$$

$$= \frac{w}{8\mu_0}\mathbf{F}(\pi)$$

$$= \frac{w}{8\mu_0}\operatorname{diag}[F_{11}(\pi); F_{22}(\pi); F_{33}(\pi); F_{44}(\pi)]$$

$$= \frac{w}{8\mu_0}\operatorname{diag}[F_{11}(\pi); F_{22}(\pi); -F_{22}(\pi); F_{11}(\pi) - 2F_{22}(\pi)]. \tag{42}$$

Furthermore, for spherical particles

$$\mathbf{S}^1(\mu_0, \mu_0, \pi) = \operatorname{diag}[S_{11}^1(\mu_0, \mu_0, \pi); S_{11}^1(\mu_0, \mu_0, \pi); -S_{11}^1(\mu_0, \mu_0, \pi); -S_{11}^1(\mu_0, \mu_0, \pi)]$$

$$= \frac{w}{8\mu_0}\operatorname{diag}[F_{11}(\pi); F_{11}(\pi); -F_{11}(\pi); -F_{11}(\pi)] \tag{43}$$

[cf. Eqs. (39) and (40)]. The ladder component of the reflection matrix for exactly the backscattering direction is computed as

$$\mathbf{S}^{\mathrm{L}}(\mu_0, \mu_0, \pi) = \mathbf{R}(\mu_0, \mu_0, \pi) - \mathbf{S}^{\mathrm{I}}(\mu_0, \mu_0, \pi). \tag{44}$$

Finally, the cyclical component for exactly the backscattering direction is computed using Eqs. (11)–(15).

The calculational method described and the corresponding computer code are extremely efficient so that the CPU time for calculating one scattering model on an IBM RISC model 37T workstation is of the order of 1 min. The computer code is available from the author upon request (e-mail: crmim@nasagiss.giss.nasa.gov).

3. RADAR REFLECTIVITY, POLARIZATION RATIOS, AND ENHANCEMENT FACTORS

In most modern radar observations, the transmitted radar signal is fully linearly or circularly polarized and two parallel receiving channels are used to measure radar returns in the same linear (circular) polarization as transmitted and simultaneously in the opposite sense.[17] The Stokes representation of polarization introduced in the previous section is not quite suitable to describe situations involving radar measurements. Therefore, it is convenient to introduce two other representations, so-called modified Stokes (MS) and circular-polarization (CP) representations, given by[18,43,52]

$$\mathbf{I}^{\mathrm{MS}} = \begin{bmatrix} I_{\mathrm{v}} \\ I_{\mathrm{h}} \\ U \\ V \end{bmatrix} = \begin{bmatrix} \frac{1}{2}(I+Q) \\ \frac{1}{2}(I-Q) \\ U \\ V \end{bmatrix} = \mathbf{B}\mathbf{I} \tag{45}$$

and

$$\mathbf{I}^{\mathrm{CP}} = \frac{1}{2} \begin{bmatrix} Q + iU \\ I + V \\ I - V \\ Q - iU \end{bmatrix} = \mathbf{A}\mathbf{I}, \tag{46}$$

respectively, where

$$\mathbf{B} = \begin{bmatrix} \frac{1}{2} & \frac{1}{2} & 0 & 0 \\ \frac{1}{2} & -\frac{1}{2} & 0 & 0 \\ 0 & 0 & 1 & 0 \\ 0 & 0 & 0 & 1 \end{bmatrix}, \tag{47}$$

$$\mathbf{A} = \frac{1}{2} \begin{bmatrix} 0 & 1 & i & 0 \\ 1 & 0 & 0 & 1 \\ 1 & 0 & 0 & -1 \\ 0 & 1 & -i & 0 \end{bmatrix}. \tag{48}$$

Conversely, we have

$$\mathbf{I} = \mathbf{B}^{-1}\mathbf{I}^{\mathrm{MS}}, \tag{49}$$

$$\mathbf{I} = \mathbf{A}^{-1}\mathbf{I}^{\mathrm{CP}}, \tag{50}$$

where

$$\mathbf{B}^{-1} = \begin{bmatrix} 1 & 1 & 0 & 0 \\ 1 & -1 & 0 & 0 \\ 0 & 0 & 1 & 0 \\ 0 & 0 & 0 & 1 \end{bmatrix}, \tag{51}$$

$$\mathbf{A}^{-1} = \begin{bmatrix} 0 & 1 & 1 & 0 \\ 1 & 0 & 0 & 1 \\ -i & 0 & 0 & i \\ 0 & 1 & -1 & 0 \end{bmatrix}. \tag{52}$$

Denoting the reflection matrix in these two new representations of polarization by $\mathbf{M}(\mu, \mu_0, \varphi - \varphi_0)$ and $\mathbf{C}(\mu, \mu_0, \varphi - \varphi_0)$, respectively, and using Eqs. (9), (45), (46), (49), and (50), we easily derive:

$$\mathbf{M}(\mu, \mu_0, \varphi - \varphi_0) = \mathbf{BS}(\mu, \mu_0, \varphi - \varphi_0)\mathbf{B}^{-1} \tag{53}$$

and[43]

$$\mathbf{C}(\mu, \mu_0, \varphi - \varphi_0) = \mathbf{AS}(\mu, \mu_0, \varphi - \varphi_0)\mathbf{A}^{-1}. \tag{54}$$

These two simple formulas can be used to compute the matrices $\mathbf{M}(\mu, \mu_0, \varphi - \varphi_0)$ and $\mathbf{C}(\mu, \mu_0, \varphi - \varphi_0)$ after the Stokes reflection matrix $\mathbf{S}(\mu, \mu_0, \varphi - \varphi_0)$ has been computed as described in the previous section.

In accordance with Refs. 18, 41, and 52, we define the radar backscattering coefficients in the modified Stokes and circular polarization representations as

$$\boldsymbol{\sigma}^{\mathrm{MS}}(\mu_0) = 4\mu_0^2\mathbf{M}(\mu_0, \mu_0, \pi) = 4\mu_0^2\mathbf{BS}(\mu_0, \mu_0, \pi)\mathbf{B}^{-1} \tag{55}$$

and

$$\boldsymbol{\sigma}^{\mathrm{CP}}(\mu_0) = 4\mu_0^2\mathbf{C}(\mu_0, \mu_0, \pi) = 4\mu_0^2\mathbf{AS}(\mu_0, \mu_0, \pi)\mathbf{A}^{-1}, \tag{56}$$

respectively. Consider first the case when the transmitted radar signal is linearly polarized in the vertical direction so that $\mathbf{I}_0^{\mathrm{MS}} = [I_{v0}, 0, 0, 0]^{\mathrm{T}}$, where T denotes matrix transpose. The vertically and horizontally polarized components of the received signal at exactly the backscattering direction are described by the co-polarized and cross-polarized radar reflectivities given by the (1,1) and (2,1) elements of the matrix $\boldsymbol{\sigma}^{\mathrm{MS}}(\mu_0)$, respectively:

$$\sigma_{\mathrm{vv}}(\mu_0) = \sigma_{11}^{\mathrm{MS}}(\mu_0), \tag{57}$$

$$\sigma_{\mathrm{hv}}(\mu_0) = \sigma_{21}^{\mathrm{MS}}(\mu_0). \tag{58}$$

The linear polarization ratio is defined as the ratio of the cross-polarized to the co-polarized radar reflectivities:

$$\mu_{\mathrm{L}}(\mu_0) = \frac{\sigma_{\mathrm{hv}}(\mu_0)}{\sigma_{\mathrm{vv}}(\mu_0)}. \tag{59}$$

Similarly, for a transmitted radar signal with right-circular polarization, $\mathbf{I}_0^{\mathrm{CP}} = [0, I_0^{\mathrm{CP}}, 0, 0]^{\mathrm{T}}$, the same-circular and opposite-circular radar reflectivities and the circular polarization ratio are given by

$$\sigma_{\mathrm{SC}}(\mu_0) = \sigma_{22}^{\mathrm{CP}}(\mu_0), \tag{60}$$

$$\sigma_{\mathrm{OC}}(\mu_0) = \sigma_{32}^{\mathrm{CP}}(\mu_0), \tag{61}$$

and

$$\mu_{\mathrm{C}}(\mu_0) = \frac{\sigma_{\mathrm{SC}}(\mu_0)}{\sigma_{\mathrm{OC}}(\mu_0)}, \tag{62}$$

respectively. Assuming spherical scatterers and using Eqs. (10)–(15), (17), (43), (55), and (56), the radar reflectivities can be expressed in the elements of the Stokes reflection matrix as follows:

$$\sigma_{\mathrm{vv}}(\mu_0) = 4\mu_0^2[S_{11}^{\mathrm{I}}(\mu_0, \mu_0, \pi) + S_{11}^{\mathrm{L}}(\mu_0, \mu_0, \pi) + 2S_{12}^{\mathrm{L}}(\mu_0, \mu_0, \pi) + S_{22}^{\mathrm{L}}(\mu_0, \mu_0, \pi)], \tag{63}$$

$$\sigma_{\mathrm{hv}}(\mu_0) = 2\mu_0^2[S_{11}^{\mathrm{L}}(\mu_0, \mu_0, \pi) - S_{22}^{\mathrm{L}}(\mu_0, \mu_0, \pi) - S_{33}^{\mathrm{L}}(\mu_0, \mu_0, \pi) + S_{44}^{\mathrm{L}}(\mu_0, \mu_0, \pi)], \tag{64}$$

$$\sigma_{\mathrm{SC}}(\mu_0) = 4\mu_0^2[S_{11}^{\mathrm{L}}(\mu_0, \mu_0, \pi) + S_{44}^{\mathrm{L}}(\mu_0, \mu_0, \pi)], \tag{65}$$

$$\sigma_{OC}(\mu_0) = 2\mu_0^2[2S_{11}^{I}(\mu_0, \mu_0, \pi) + S_{11}^{L}(\mu_0, \mu_0, \pi) + S_{22}^{L}(\mu_0, \mu_0, \pi) - S_{33}^{L}(\mu_0, \mu_0, \pi) - S_{44}^{L}(\mu_0, \mu_0, \pi)]. \quad (66)$$

In the vicinity of the exact backscattering direction but outside the coherent backscattering peak, the cyclical contribution to the radar reflectivities vanishes, while the diffuse contribution is given by

$$\sigma_{vv}^{diff}(\mu_0) = 4\mu_0^2[S_{11}^{I}(\mu_0, \mu_0, \pi) + \tfrac{1}{2}S_{11}^{L}(\mu_0, \mu_0, \pi) + S_{12}^{L}(\mu_0, \mu_0, \pi) + \tfrac{1}{2}S_{22}^{L}(\mu_0, \mu_0, \pi)], \quad (67)$$

$$\sigma_{hv}^{diff}(\mu_0) = 2\mu_0^2[S_{11}^{L}(\mu_0, \mu_0, \pi) - S_{22}^{L}(\mu_0, \mu_0, \pi)], \quad (68)$$

$$\sigma_{SC}^{diff}(\mu_0) = 2\mu_0^2[S_{11}^{L}(\mu_0, \mu_0, \pi) + S_{44}^{L}(\mu_0, \mu_0, \pi)], \quad (69)$$

$$\sigma_{OC}^{diff}(\mu_0) = 2\mu_0^2[2S_{11}^{I}(\mu_0, \mu_0, \pi) + S_{11}^{L}(\mu_0, \mu_0, \pi) - S_{44}^{L}(\mu_0, \mu_0, \pi)]. \quad (70)$$

The corresponding diffuse polarization ratios are

$$\mu_L^{diff}(\mu_0) = \frac{\sigma_{hv}^{diff}(\mu_0)}{\sigma_{vv}^{diff}(\mu_0)} \quad (71)$$

and

$$\mu_C^{diff}(\mu_0) = \frac{\sigma_{SC}^{diff}(\mu_0)}{\sigma_{OC}^{diff}(\mu_0)}. \quad (72)$$

We also define backscattering enhancement factors as ratios of full radar reflectivities to respective diffuse radar reflectivities:

$$\zeta_{vv}(\mu_0) = \frac{\sigma_{vv}(\mu_0)}{\sigma_{vv}^{diff}(\mu_0)}, \quad (73)$$

$$\zeta_{hv}(\mu_0) = \frac{\sigma_{hv}(\mu_0)}{\sigma_{hv}^{diff}(\mu_0)}, \quad (74)$$

$$\zeta_{SC}(\mu_0) = \frac{\sigma_{SC}(\mu_0)}{\sigma_{SC}^{diff}(\mu_0)}, \quad (75)$$

$$\zeta_{OC}(\mu_0) = \frac{\sigma_{OC}(\mu_0)}{\sigma_{OC}^{diff}(\mu_0)}. \quad (76)$$

The backscattering enhancement factors possess several interesting properties.[12] As follows from Eqs. (65), (69), and (75), the same-circular enhancement factor for spherical particles is identically equal to 2:

$$\zeta_{SC}(\mu_0) \equiv 2. \quad (77)$$

This identity is a direct consequence of Eq. (43) and, in general, does not hold for nonspherical particles.[24] Using the Newmann order-of-scattering expansion of Eq. (21) in powers of w and taking into account Eq. (44), it is easy to show that with decreasing single scattering albedo the ladder component of the Stokes reflection matrix $\mathbf{S}^{L}(\mu, \mu_0, \varphi - \varphi_0)$ decreases and ultimately vanishes. Therefore, it follows from Eqs. (63), (66), (67), (70), (73), and (76) that

$$\lim_{w \to 0} \zeta_{vv}(\mu_0) = \lim_{w \to 0} \zeta_{OC}(\mu_0) = 1. \quad (78)$$

Also, in grazing incidence and reflection (i.e., in the limit $\mu \to 0$ and $\mu_0 \to 0$), the diffuse reflection matrix $\mathbf{R}(\mu, \mu_0, \varphi - \varphi_0)$ becomes equal to the first-order-scattering component $\mathbf{S}^{I}(\mu, \mu_0, \varphi - \varphi_0)$ (see Sec. 15.3.5 of Ref. 47), which means that the ladder component $\mathbf{S}^{L}(\mu, \mu_0, \varphi - \varphi_0)$ vanishes [cf. Eq. (44)]. As a consequence, we easily derive from Eqs. (63), (66), (67), (70), (73), and (76):

$$\lim_{\mu_0 \to 0} \zeta_{vv}(\mu_0) = \lim_{\mu_0 \to 0} \zeta_{OC}(\mu_0) = 1. \quad (79)$$

Finally, useful upper and lower bounds for the backscattering enhancement factors can be derived by employing the general inequalities that must be satisfied by any Stokes transformation matrix

of the block-diagonal form given by Eq. (17) (see Sec. 3.3 of Ref. 53). Applying these inequalities to the matrix $\mathbf{S}^{L}(\mu_0, \mu_0, \pi)$, we easily derive from Eqs. (63), (64), (66), (73), (74), and (76):[24]

$$1 \leqslant \zeta_{vv}(\mu_0) \leqslant 2, \tag{80}$$

$$0 \leqslant \zeta_{hv}(\mu_0) \leqslant 2, \tag{81}$$

$$0 \leqslant \zeta_{oc}(\mu_0) \leqslant 2. \tag{82}$$

Similar inequalities and asymptotic limits can be derived for the polarization ratios:

$$\mu_{pol}(\mu_0) \geqslant 0, \tag{83}$$

$$\lim_{w \to 0} \mu_{pol}(\mu_0) = \lim_{\mu_0 \to 0} \mu_{pol}(\mu_0) = 0, \tag{84}$$

where μ_{pol} stands for μ_L, μ_C, μ_L^{diff}, or μ_C^{diff}. It should be emphasized, however, that Eq. (84) is a specific property of spherical particles and does not hold for nonspherical scatterers.

4. CALCULATIONS AND DISCUSSION

All numerical results reported below have been computed for polydisperse spherical particles using the standard gamma distribution of particle radii given by[31]

$$n(r) = Cr^{(1-3b)/b} \exp\left(-\frac{r}{ab}\right). \tag{85}$$

Here, $n(r)dr$ is the fraction of particles with radii from r to $r + dr$, a and b are formal model parameters, and

$$C = \frac{1}{\Gamma\left(\frac{1-2b}{b}\right)} (ab)^{(2b-1)/b}. \tag{86}$$

This choice of the constant C ensures the normalization

$$\int_0^\infty dr n(r) = 1. \tag{87}$$

The gamma distribution is very convenient in theoretical computations since its formal parameters a and b coincide with the effective radius r_{eff} and effective variance v_{eff} of the distribution, respectively, so that[31]

$$r_{eff} = \frac{1}{G} \int_0^\infty dr \pi r^3 n(r) \equiv a, \tag{88}$$

$$v_{eff} = \frac{1}{G r_{eff}^2} \int_0^\infty dr (r - r_{eff})^2 \pi r^2 n(r) \equiv b. \tag{89}$$

In Eqs. (88) and (89), G is the average particle geometric cross-sectional area given by

$$G = \int_0^\infty dr \pi r^2 n(r). \tag{90}$$

As follows from the electromagnetic theory,[45] all scattering properties of polydisperse particles depend on the effective radius r_{eff} and the wavelength of the incident radiation λ only through their ratio or, more specifically, through the effective size parameter defined as $x_{eff} = 2\pi r_{eff}/\lambda$. Figure 4

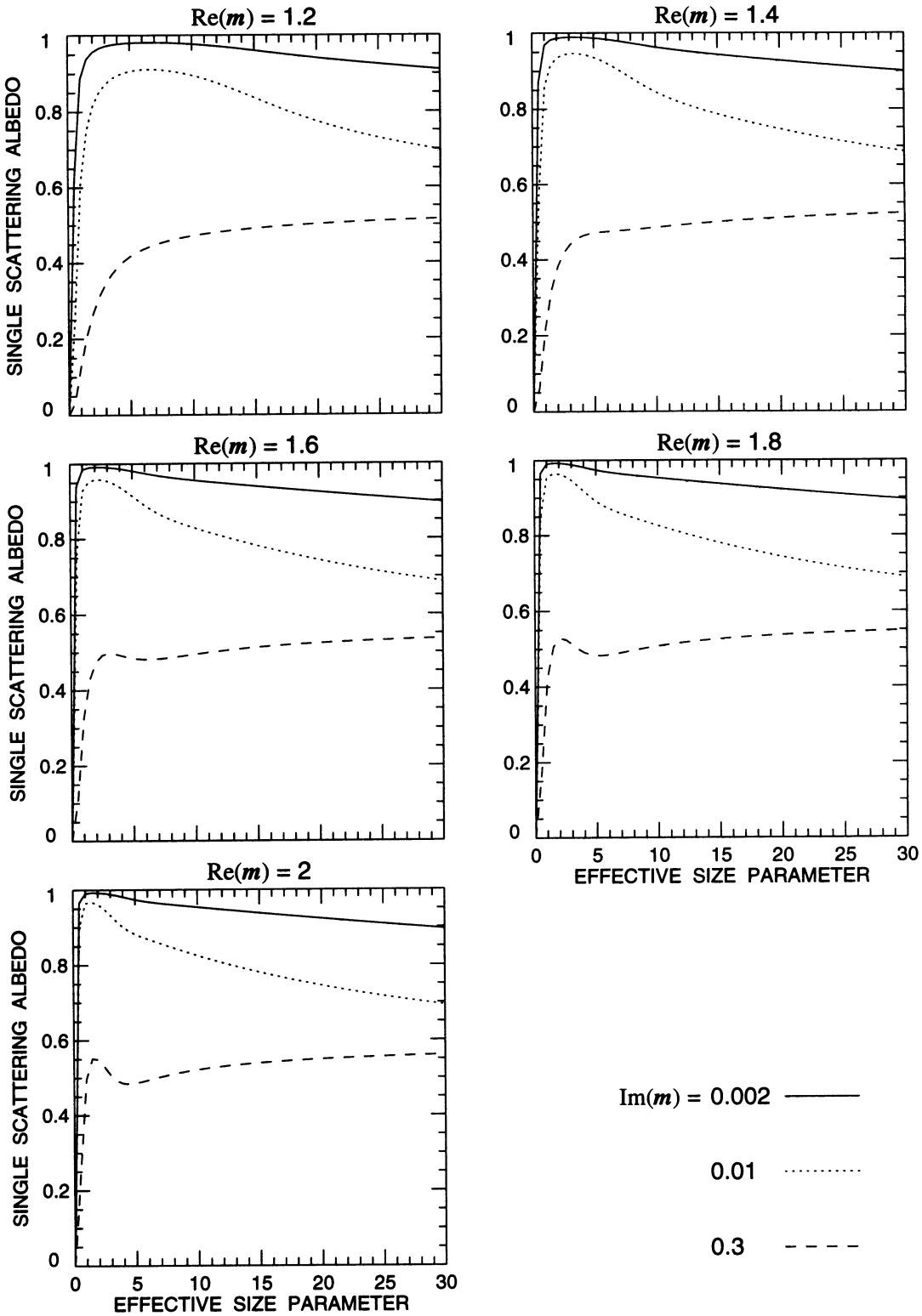

Fig. 4. Single scattering albedo w vs effective size parameter x_{eff} for polydisperse spherical particles with $v_{\text{eff}} = 0.1$, Re(m) = 1.2, 1.4, 1.6, 1.8, and 2, and Im(m) = 0.002, 0.01, and 0.3. Note that $w \equiv 1$ for nonabsorbing particles with Im(m) = 0.

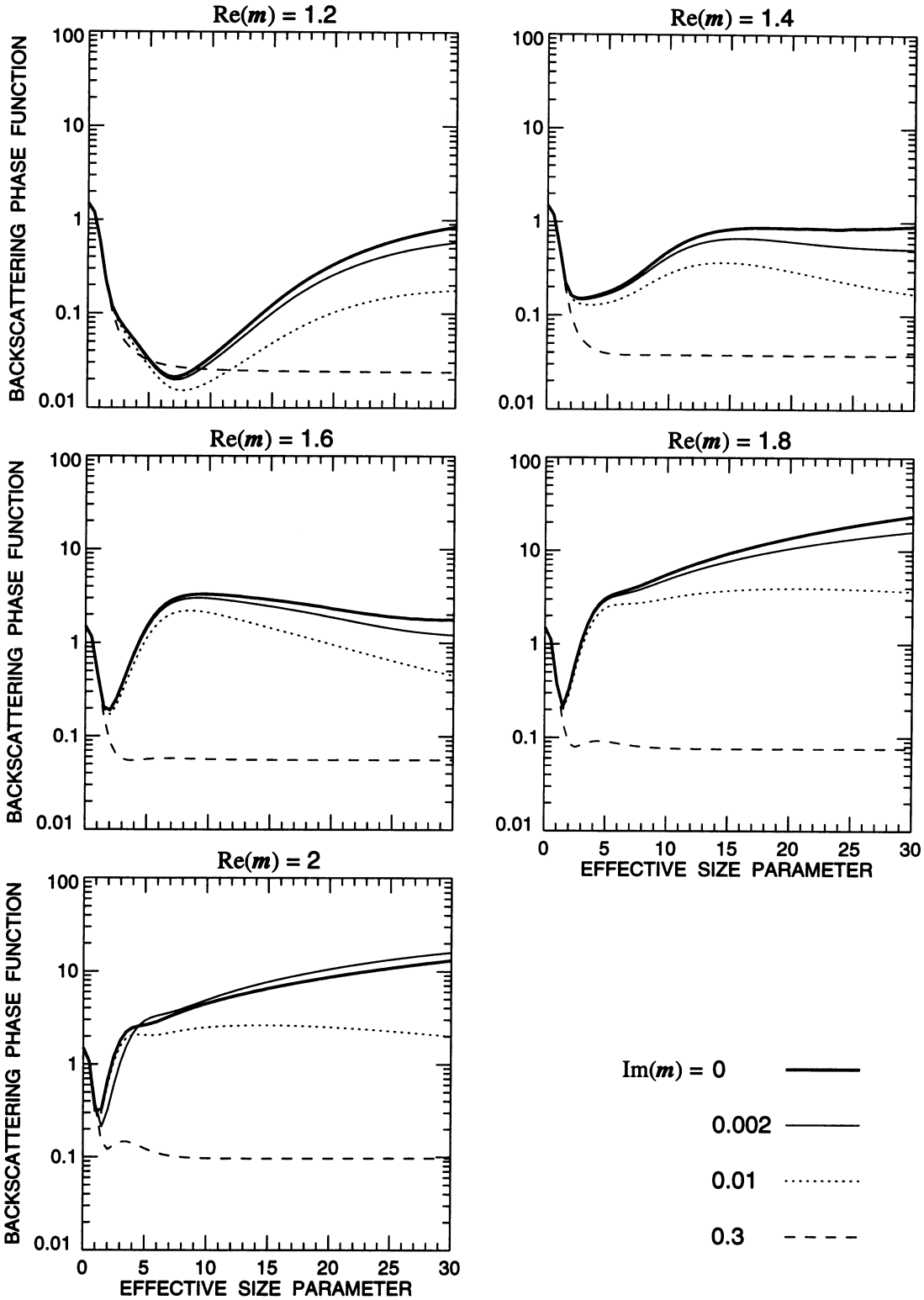

Fig. 5. Backscattering phase function $F_{11}(\pi)$ vs effective size parameter for polydisperse spherical particles with Re(m) = 1.2, 1.4, 1.6, 1.8, and 2 and Im(m) = 0, 0.002, 0.01, and 0.3.

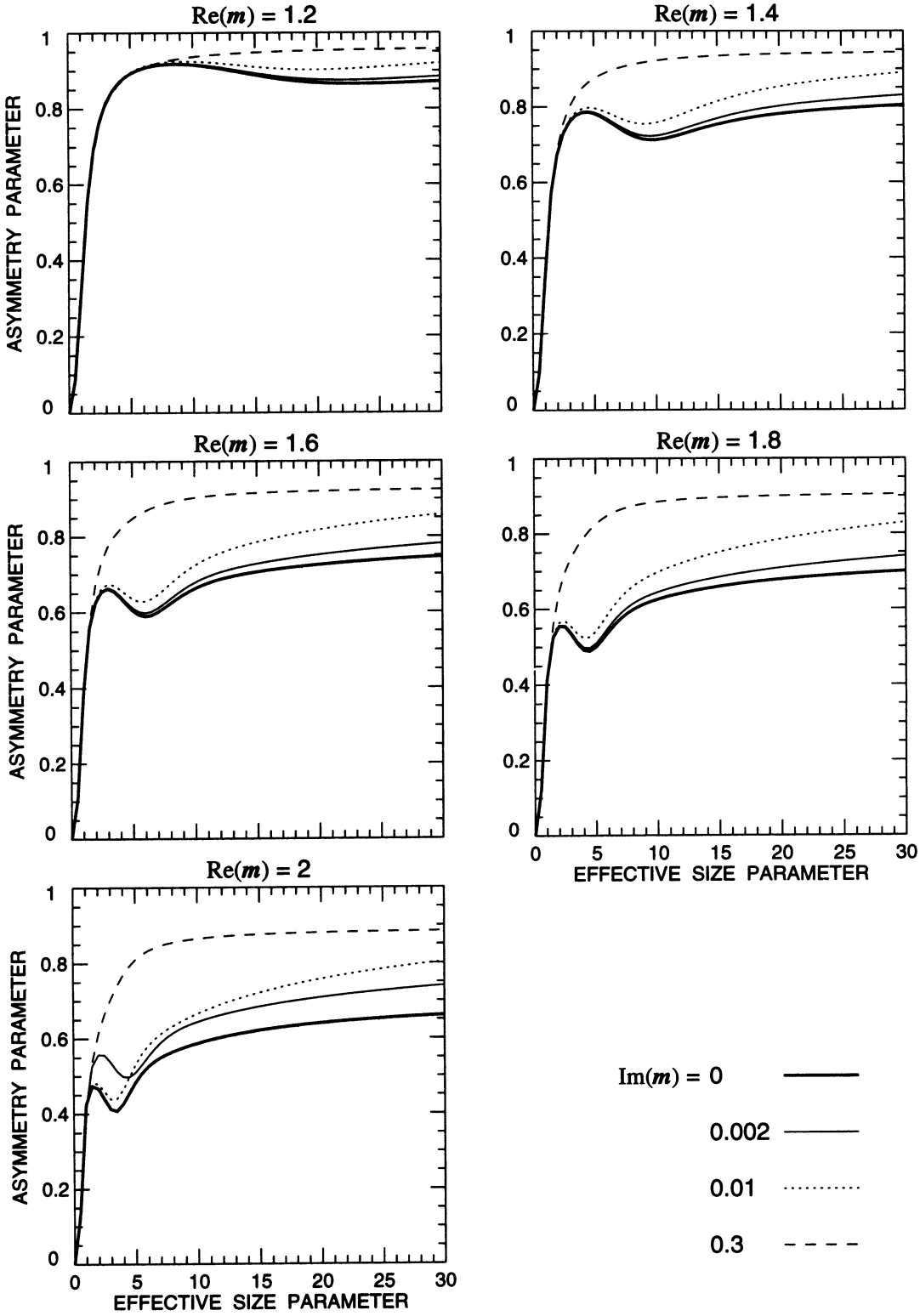

Fig. 6. Asymmetry parameter of the phase function $\langle \cos \Theta \rangle$ vs effective size parameter for polydisperse spherical particles with Re(m) = 1.2, 1.4, 1.6, 1.8, and 2 and Im(m) = 0, 0.002, 0.01, and 0.3.

shows the single-scattering albedo w vs x_{eff} ($0 \leqslant x_{\text{eff}} \leqslant 30$) for particles with $v_{\text{eff}} = 0.1$, the real part of the refractive index $\text{Re}(m) = 1.2$, 1.4, 1.6, 1.8, and 2, and the imaginary part of the refractive index $\text{Im}(m) = 0$, 0.002, 0.01, and 0.3. Note that for nonabsorbing particles [$\text{Im}(m) = 0$], w is identically equal to 1. Similarly, Fig. 5 shows the backscattering phase function $F_{11}(\pi)$ and Fig. 6 displays the asymmetry parameter of the phase function defined as

$$\langle \cos \Theta \rangle = \tfrac{1}{2} \int_{-1}^{1} \mathrm{d}(\cos \Theta) F_{11}(\Theta) \cos \Theta = \frac{a_1^1}{3}. \tag{91}$$

The asymmetry parameter is a quantitative measure of the single-scattering anisotropy and is positive for predominantly forward-scattering particles, negative for backscattering particles, and vanishes for isotropic scattering [$F_{11}(\Theta) \equiv 1$] and symmetric phase functions with $F_{11}(\pi - \Theta) = F_{11}(\Theta)$.

It is seen from Figs. 4–6 that the dependence of the three single-scattering characteristics on the imaginary part of the refractive index is rather simple. Indeed, w always decreases, $F_{11}(\pi)$ almost always decreases, and $\langle \cos \Theta \rangle$ almost always increases with increasing absorption. In the Rayleigh limit ($x_{\text{eff}} = 0$), the asymmetry parameter vanishes, the backscattering phase function is equal to 1.5, and the single-scattering albedo is equal to zero [except for $\text{Im}(m) = 0$] regardless of the real part of the refractive index. Of the three single-scattering characteristics, w is least sensitive to the real part of the refractive index. In contrast, for nonabsorbing particles with $x_{\text{eff}} = 7$ the backscattering phase function $F_{11}(\pi)$ increases by more than two orders of magnitude as $\text{Re}(m)$ increases from 1.2 to 1.6. The backscattering phase function is also most sensitive to increasing absorption. For particles with $\text{Re}(m) = 1.8$ and $x_{\text{eff}} = 30$, $F_{11}(\pi)$ drops by more than two orders of magnitude with increasing imaginary part of the refractive index from 0 to 0.3, thus demonstrating the strong suppressing effect of absorption on glory. The minimum in the backscattering phase function curves for $\text{Im}(m) = 0$, 0.002, and 0.01 shifts towards smaller effective size parameters and becomes shallower with increasing $\text{Re}(m)$. The minimum disappears for $\text{Im}(m) = 0.3$ as the real part of the refractive index becomes smaller than about 1.5. For $\text{Im}(m) = 0.3$ and effective size parameters greater than about 8, the backscattering phase function and the asymmetry parameter curves become essentially independent of x_{eff}. Importantly, our computations show that an increase of the backscattering phase function with increasing x_{eff} is not necessarily accompanied by a decrease of the asymmetry parameter, as it is sometimes implied (e.g., Ref. 54).

Plates 1–8 are composed of color contour diagrams of the photometric and polarimetric characteristics of a radar return as functions of the effective size parameter x_{eff} and the cosine of the illumination zenith angle μ_0 for the same values of the real [$\text{Re}(m) = 1.2$, 1.4, 1.6, 1.8, and 2] and imaginary [$\text{Im}(m) = 0$, 0.002, 0.02, and 0.3] parts of the refractive index. Plate 1 and analogous computations for the copolarized radar reflectivity σ_{vv} (not shown) demonstrate that for all x_{eff} and $\text{Re}(m)$, the effect of increasing imaginary part of the refractive index on both σ_{vv} and σ_{OC} is significant and results in strongly reduced reflectance. Figures 4, 5, and 6 suggest that this effect is caused by three factors. First, the contribution of n times scattered photons to the reflected intensity is proportional to the nth power of the single scattering albedo.[47] Therefore, the decrease of w with increasing absorption (Fig. 4) greatly decreases the contribution of multiply scattered light to the reflectivity of the medium. Second, increasing $\text{Im}(m)$ almost always results in greater values of the asymmetry parameter (Fig. 6), thus making the phase function more forward-scattering. Therefore, an incident photon has a greater probability of being scattered in the forward direction and needs to undergo more scattering events to exit the medium. This increases the photon scattering path length inside the medium and, thus, the probability that the photon will be absorbed before it escapes the medium. Third, increasing $\text{Im}(m)$ strongly suppresses the backscattering phase function (Fig. 5) and, thus, the first-order-scattering component of the (1,1)-element of the Stokes reflection matrix [Eq. (43)]. This third factor is especially important for large particles with a large real part of the refractive index and/or for nearly grazing incidence (small μ_0), in which cases the relative contribution of the first-order-scattering component to the total reflectivity for nonabsorbing particles is significant and sometimes dominant. The first two factors dominate for particles with smaller values of $\text{Re}(m)$ and for nearly perpendicular

illumination directions, in which cases the first-order-scattering contribution to the total reflectance for nonabsorbing particles is relatively weak and reflectivity is dominated by the multiple-scattering contribution.

Plate 2 shows that the linear polarization ratio of the diffuse background $\mu_L^{diff}(\mu_0)$ always decreases with increasing absorption. According to Eq. (68), the first-order-scattering contribution to $\sigma_{hv}^{diff}(\mu_0)$ for spherical particles is identically equal to zero. Therefore, the decrease of $\mu_L^{diff}(\mu_0)$ with increasing Im(m) might be explained by the decreased contribution of multiple scattering to $\sigma_{hv}^{diff}(\mu_0)$. However, this simple qualitative explanation does not quite work in the case of the circular polarization ratio of the diffuse background $\mu_C^{diff}(\mu_0)$ (Plate 3), even though the first-order-scattering contribution to $\sigma_{SC}^{diff}(\mu_0)$ is also equal to zero [Eq. (69)]. Indeed, diagrams for Re(m) = 1.2 and 1.4 in Plate 3 show that $\mu_C^{diff}(\mu_0)$ can first increase with increasing imaginary part of the refractive index and then rapidly decrease. This different behavior of $\mu_L^{diff}(\mu_0)$ and $\mu_C^{diff}(\mu_0)$ with increasing absorption can only be explained by the fact that different elements of the Stokes reflection matrix are involved and that the process of multiple scattering of polarized light is extremely complicated, thus necessitating the use of a rigorous approach in theoretical computations. Our calculations displayed in Plates 2 and 3 and pertaining to a representative, albeit restricted, domain of effective size parameters and real and imaginary parts of the refractive index strongly suggest that $\mu_L^{diff}(\mu_0)$ is always less than or equal to 1,

$$\mu_L^{diff}(\mu_0) \leqslant 1, \tag{92}$$

whereas $\mu_C^{diff}(\mu_0)$ can well exceed 2 and is always greater than or equal to $\mu_L^{diff}(\mu_0)$:

$$\mu_L^{diff}(\mu_0) \leqslant \mu_C^{diff}(\mu_0). \tag{93}$$

Unfortunately, we were unable to prove the inequalities of Eqs. (92) and (93) analytically.

The full linear and circular polarization ratios $\mu_L(\mu_0)$ and $\mu_C(\mu_0)$ are shown in Plates 4 and 5, respectively, and exhibit a more similar behavior than the corresponding diffuse ratios. In particular, the diagrams for Re(m) = 1.2 and 1.4 show that both $\mu_L(\mu_0)$ and $\mu_C(\mu_0)$ can first increase with increasing absorption and then rapidly decrease. Using formulas of Sec. 3, we can express the full polarization ratios in terms of the diffuse polarization ratios and the enhancement factors as follows:

$$\mu_L(\mu_0) = \frac{\zeta_{hv}(\mu_0)}{\zeta_{vv}(\mu_0)} \mu_L^{diff}(\mu_0), \tag{94}$$

$$\mu_C(\mu_0) = \frac{\zeta_{SC}(\mu_0)}{\zeta_{OC}(\mu_0)} \mu_C^{diff}(\mu_0). \tag{95}$$

The enhancement factor $\zeta_{SC}(\mu_0)$ for spherical particles is identically equal to 2 [Eq. (77)], while the enhancement factors $\zeta_{vv}(\mu_0)$, $\zeta_{hv}(\mu_0)$, and $\zeta_{OC}(\mu_0)$ are shown in Plates 6, 7, and 8, respectively, and exhibit a rather complicated dependence on the effective size parameter and real and imaginary parts of the refractive index. In view of Eqs. (77), (82), and (95), we conclude that the opposite-circular enhancement factor is always smaller or equal to the same-circular enhancement factor,

$$\zeta_{OC}(\mu_0) \leqslant \zeta_{SC}(\mu_0), \tag{96}$$

so that coherent backscattering always increases (or at least does not change) the circular polarization ratio:

$$\mu_C^{diff}(\mu_0) \leqslant \mu_C(\mu_0). \tag{97}$$

In contrast, coherent backscattering can either increase or decrease the linear polarization ratio depending on the ratio of the cross-polarized to co-polarized enhancement factors. Plates 6 and 7 show that this ratio can well be less than unity, especially for absorbing particles and/or grazing illumination directions. Thus our accurate radiative transfer computations show the limited validity of the conclusion of Ref. 9 that coherent backscattering always decreases the linear polarization ratio. The computations displayed in Plates 4 and 5 strongly suggest that the inequality of Eq. (92)

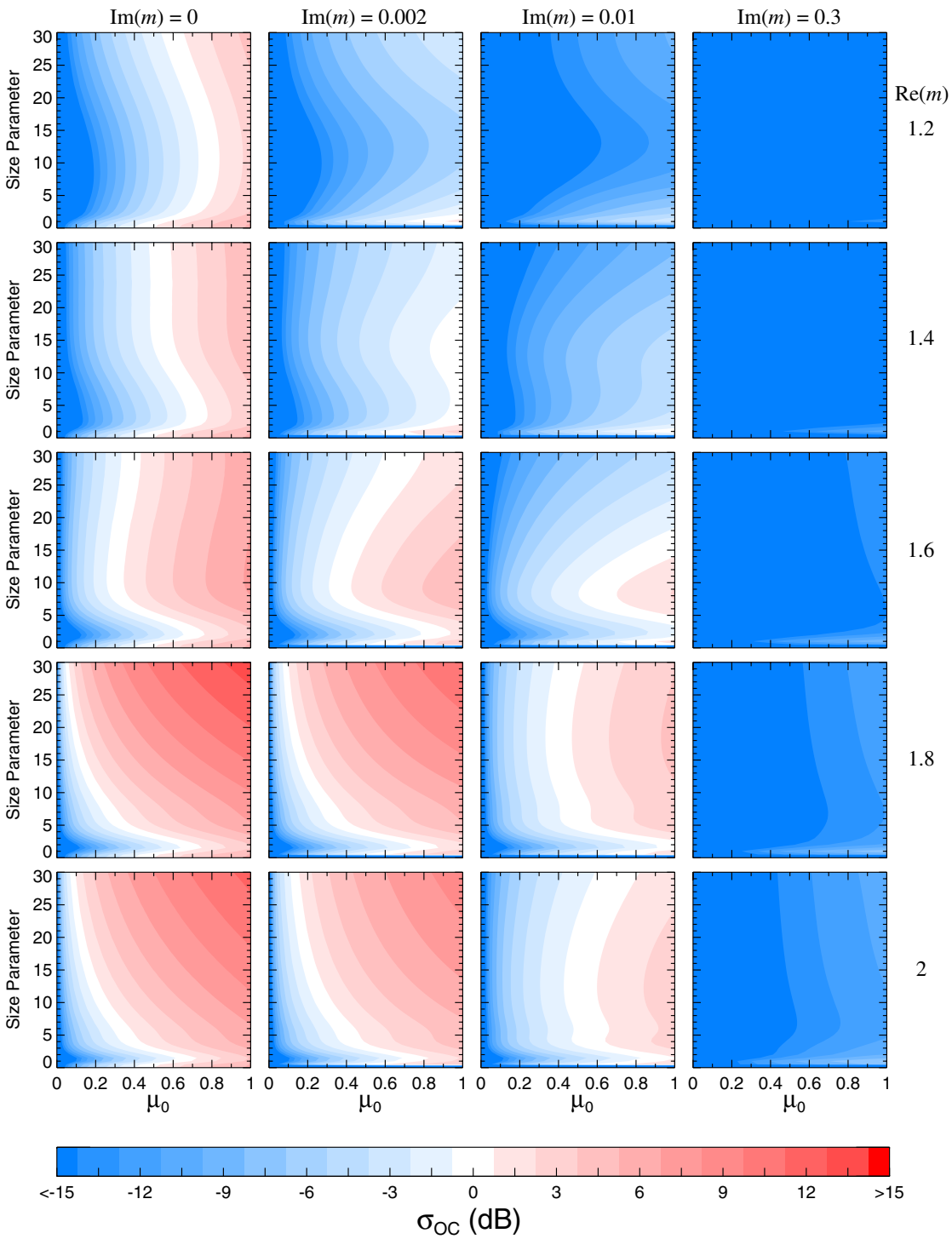

Plate 1. 10 log(σ_{OC}) (dB) vs effective size parameter x_{eff} and cosine of illumination zenith angle μ_0 for a half-space of polydisperse spherical particles with Re(m) = 1.2, 1.4, 1.6, 1.8, and 2 and Im(m) = 0, 0.002, 0.01, and 0.3.

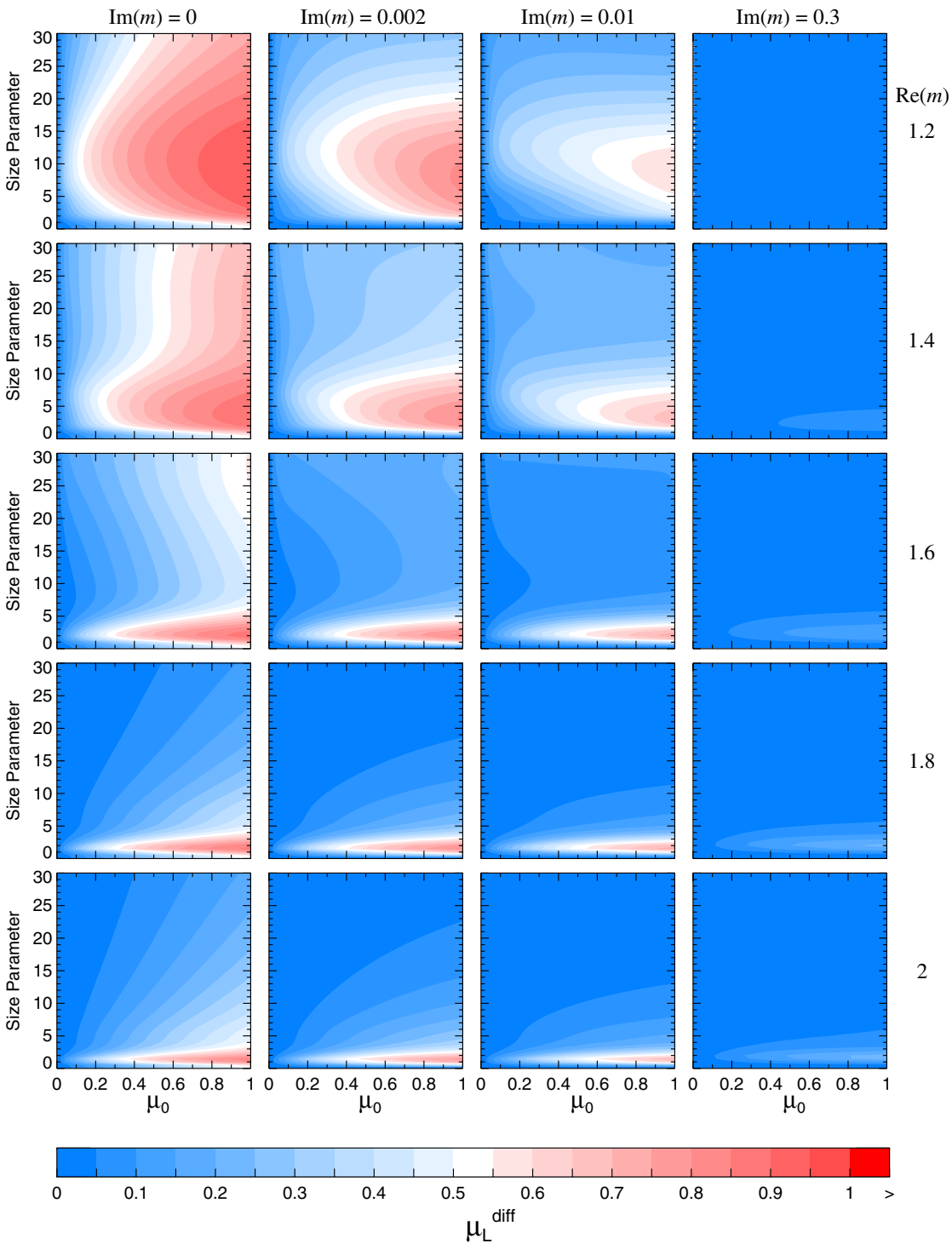

Plate 2. Linear polarization ratio of the diffuse background μ_L^{diff} vs effective size parameter x_{eff} and cosine of illumination zenith angle μ_0 for polydisperse spherical particles with Re(m) = 1.2, 1.4, 1.6, 1.8, and 2 and Im(m) = 0, 0.002, 0.01, and 0.3.

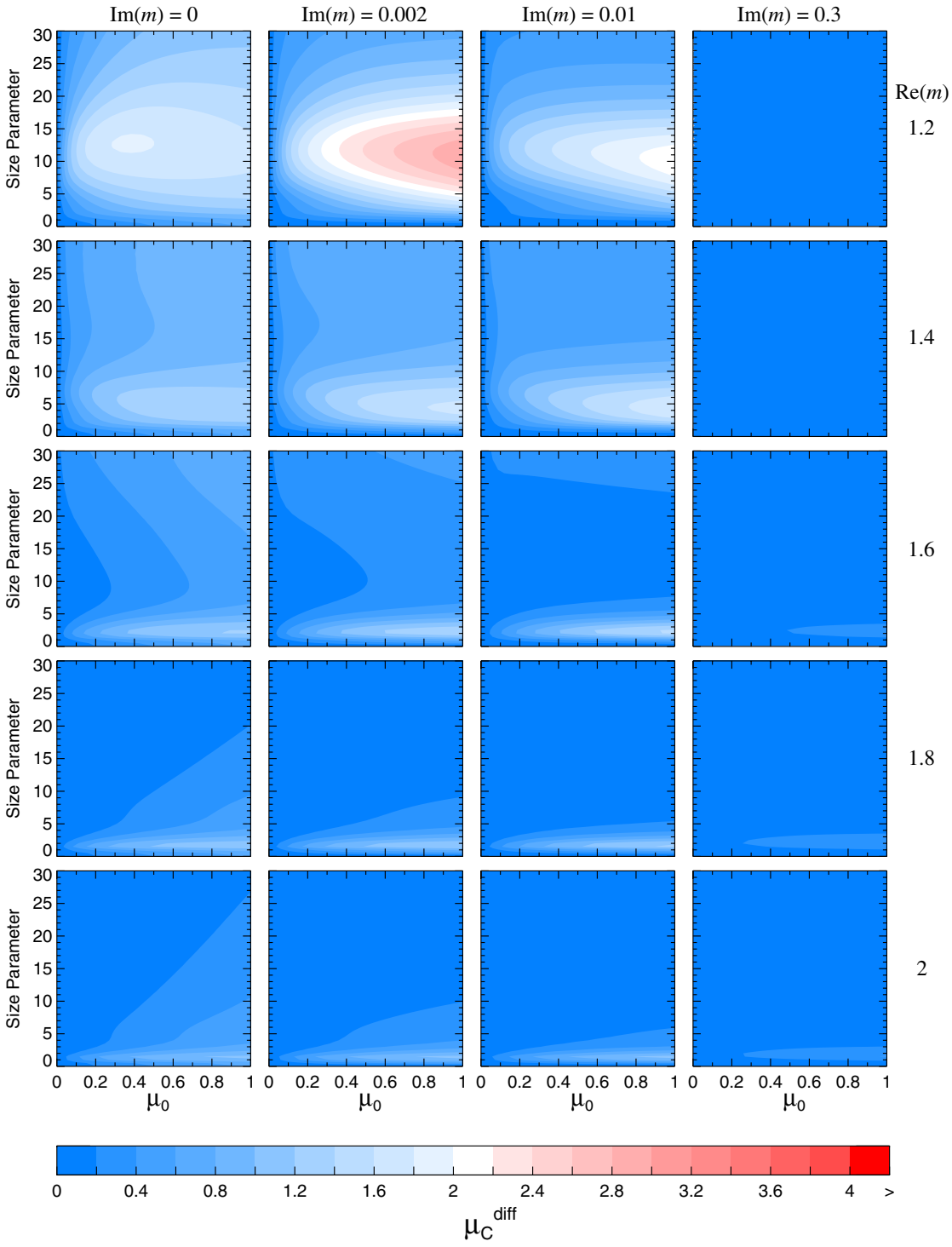

Plate 3. Circular polarization ratio of the diffuse background μ_C^{diff} vs effective size parameter x_{eff} and cosine of illumination zenith angle μ_0 for polydisperse spherical particles with Re(m) = 1.2, 1.4, 1.6, 1.8, and 2 and Im(m) = 0, 0.002, 0.01, and 0.3.

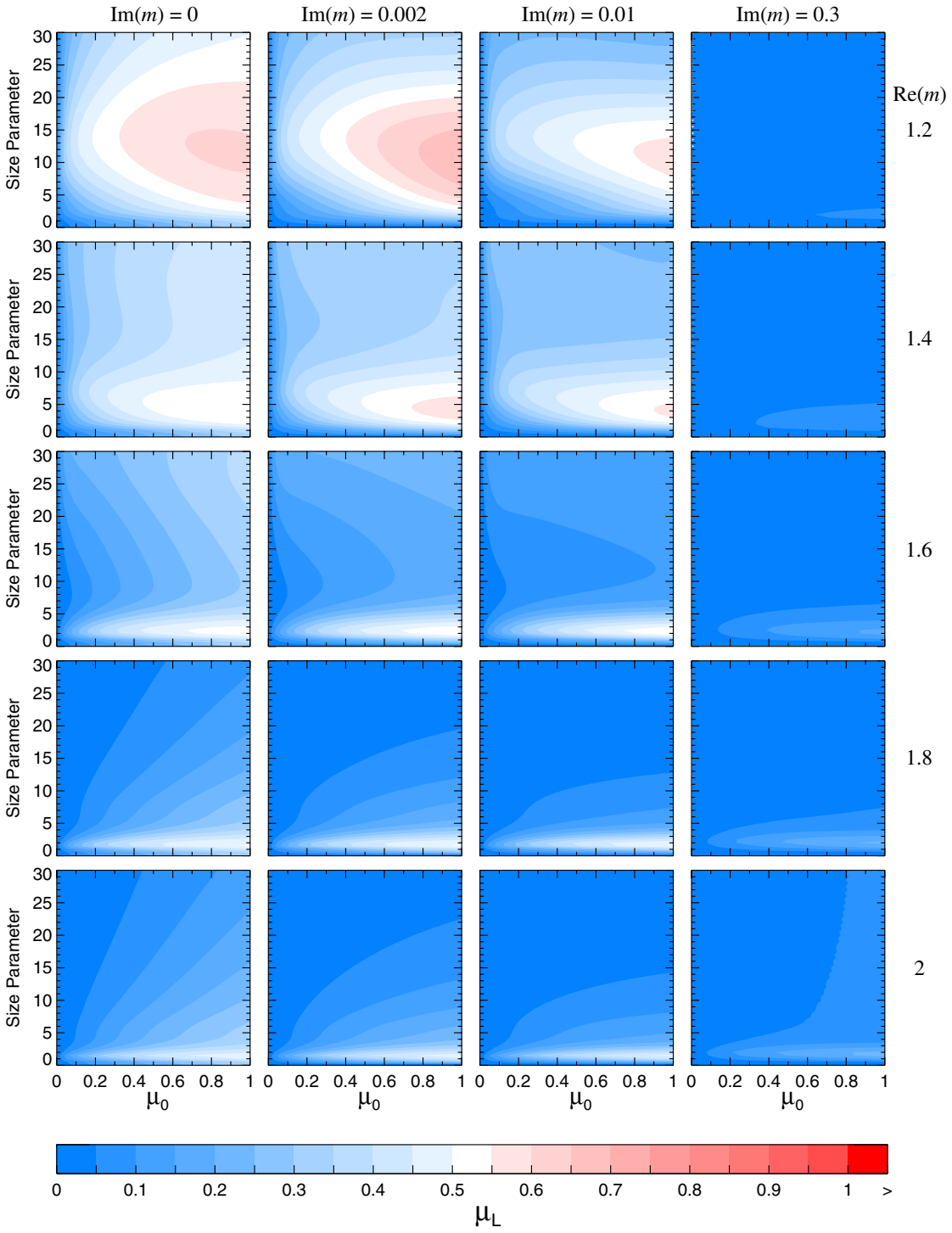

Plate 4. Linear polarization ratio μ_L vs effective size parameter x_{eff} and cosine of illumination zenith angle μ_0 for polydisperse spherical particles with Re(m) = 1.2, 1.4, 1.6, 1.8, and 2 and Im(m) = 0, 0.002, 0.01, and 0.3.

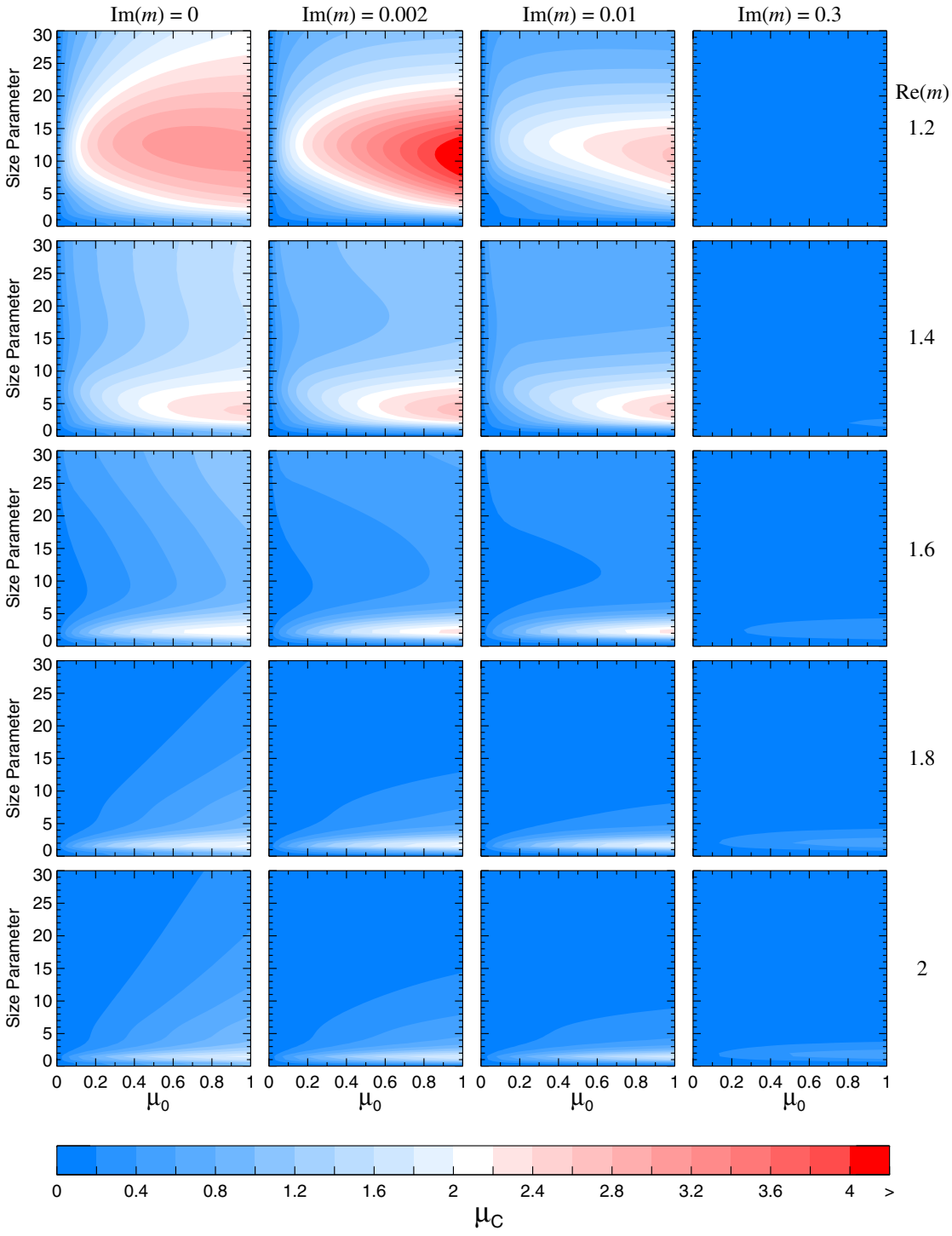

Plate 5. Circular polarization ratio μ_C vs effective size parameter x_{eff} and cosine of illumination zenith angle μ_0 for polydisperse spherical particles with Re(m) = 1.2, 1.4, 1.6, 1.8, and 2 and Im(m) = 0, 0.002, 0.01, and 0.3.

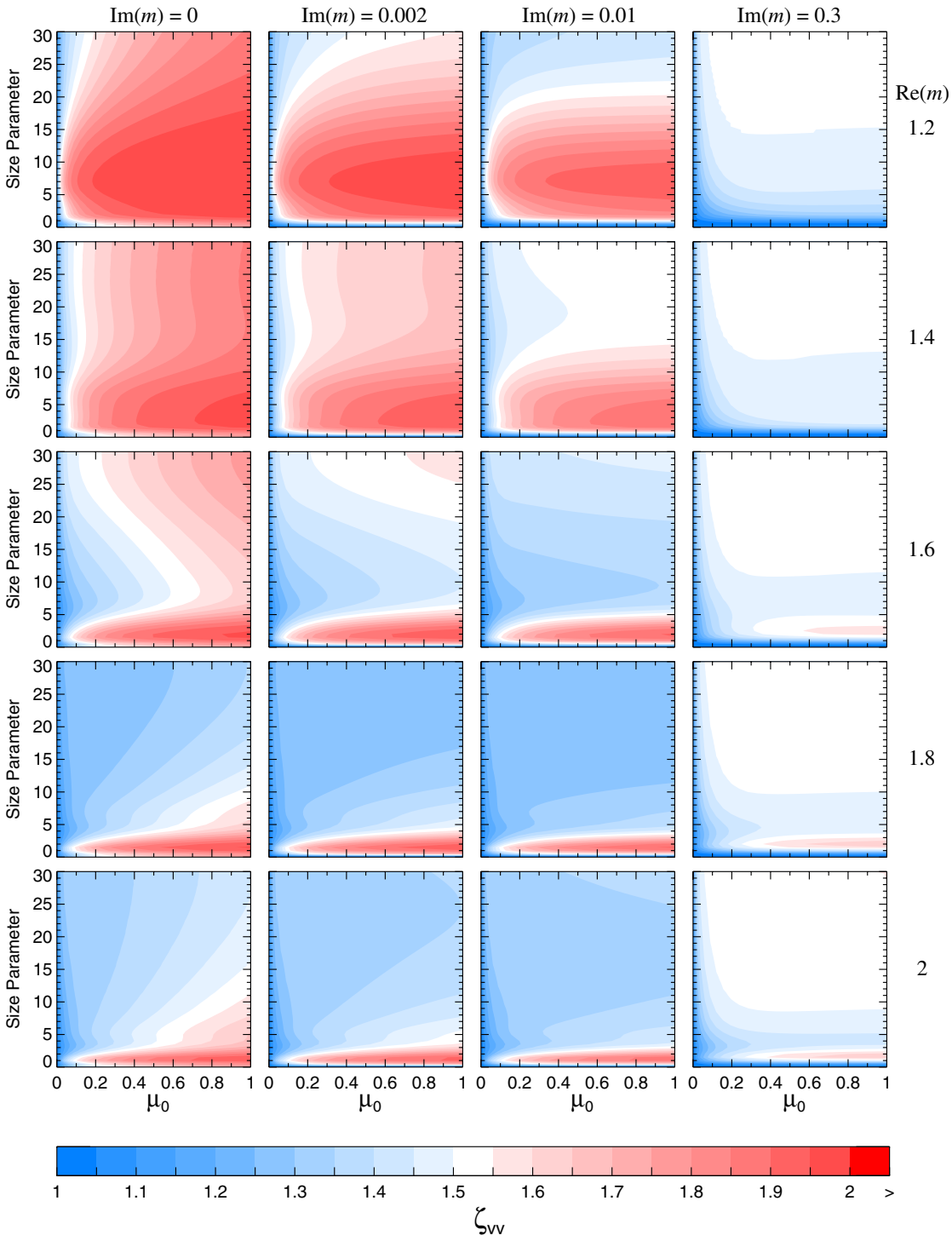

Plate 6. Copolarized backscattering enhancement factor ζ_{vv} vs effective size parameter x_{eff} and cosine of illumination zenith angle μ_0 for polydisperse spherical particles with Re(m) = 1.2, 1.4, 1.6, 1.8, and 2 and Im(m) = 0, 0.002, 0.01, and 0.3.

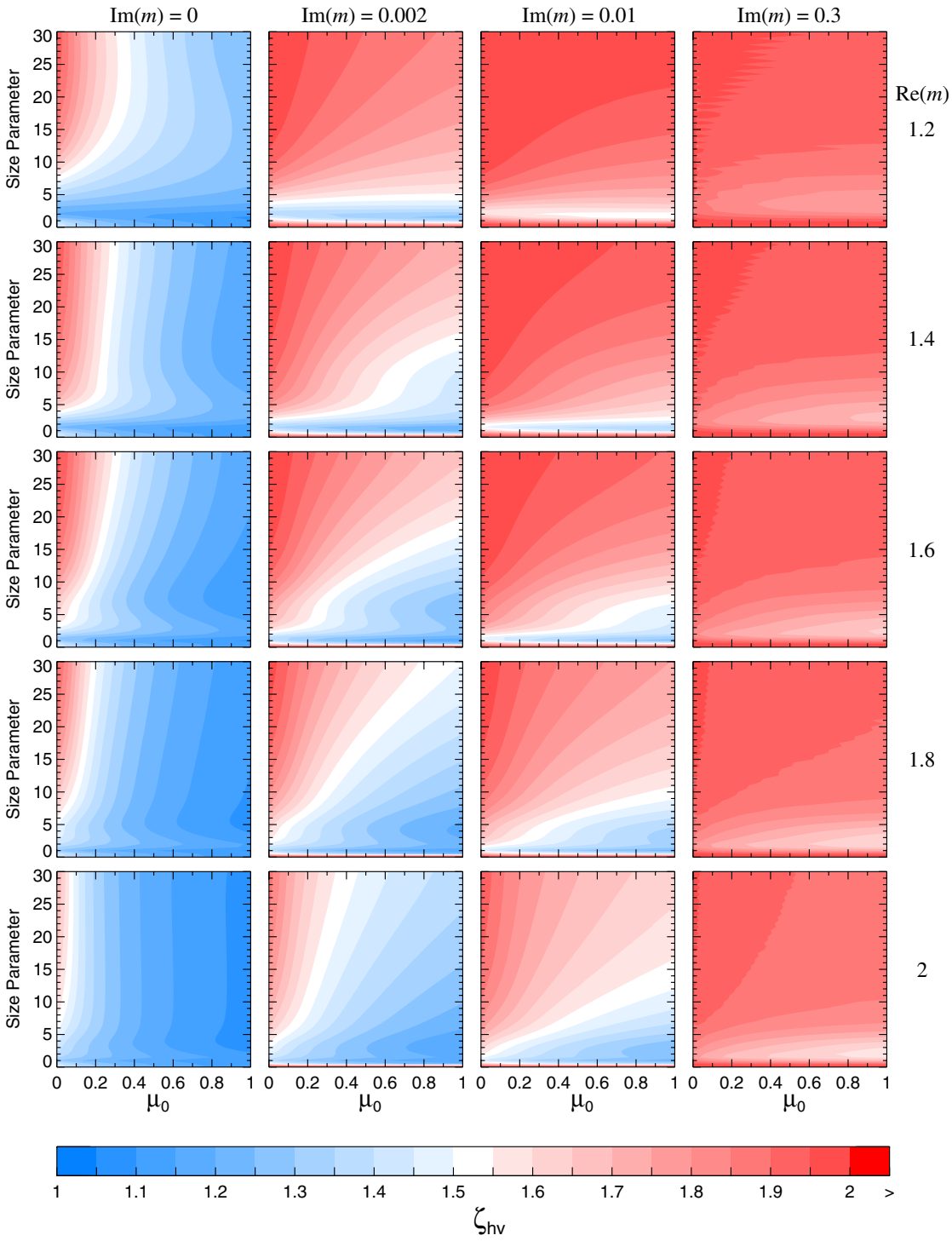

Plate 7. Cross-polarized backscattering enhancement factor ζ_{hv} vs effective size parameter x_{eff} and cosine of illumination zenith angle μ_0 for polydisperse spherical particles with Re(m) = 1.2, 1.4, 1.6, 1.8, and 2 and Im(m) = 0, 0.002, 0.01, and 0.3.

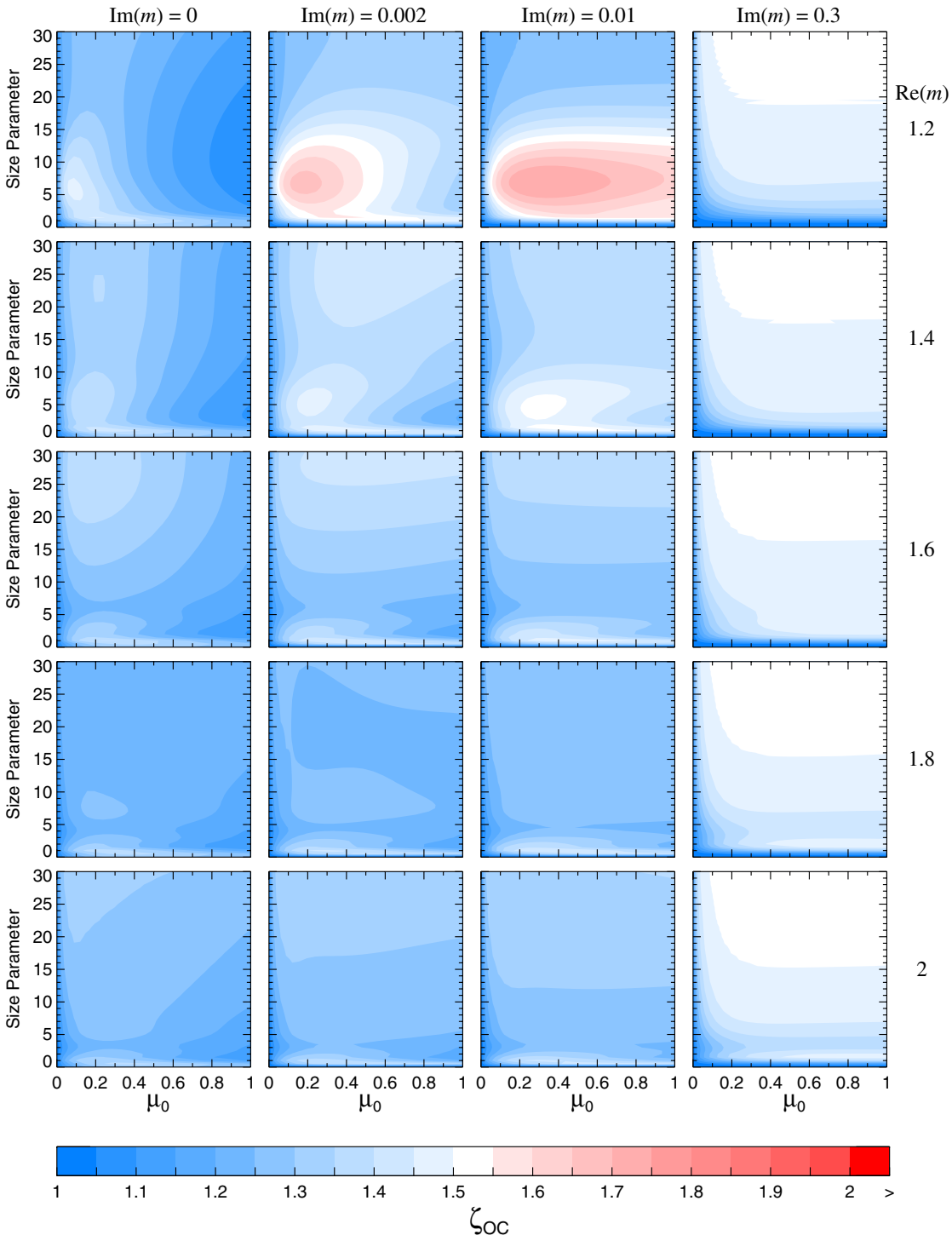

Plate 8. Opposite-circular backscattering enhancement factor ζ_{OC} vs effective size parameter x_{eff} and cosine of illumination zenith angle μ_0 for polydisperse spherical particles with Re(m) = 1.2, 1.4, 1.6, 1.8, and 2 and Im(m) = 0, 0.002, 0.01, and 0.3.

applies also to the full linear polarization ratio and that $\mu_C(\mu_0)$ is always larger than or equal to $\mu_L(\mu_0)$:

$$\mu_L(\mu_0) \leqslant 1; \quad \mu_L(\mu_0) \leqslant \mu_C(\mu_0). \tag{98}$$

Again, we were unable to prove these inequalities analytically.

As was mentioned in the Introduction, the diffusion approximation ignores the first-order-scattering contribution to the reflected light and, thus, predicts the copolarized enhancement factor exactly equal to 2.[1-3] As follows from Eqs. (63), (67), and (73), the copolarized enhancement factor is never equal to 2 since, for real scattering particles, $S_{11}^1(\mu_0, \mu_0, \pi)$ is never exactly equal to zero but rather is a positive number. Therefore, we have to conclude that for real scattering particles $\zeta_{vv}(\mu_0)$ is always smaller than 2. The degree of deviation of the copolarized enhancement factor from the value 2 strongly depends on the value of the backscattering phase function [Eqs. (43), (63), (67), and (73)]. For nonabsorbing particles with $\mathrm{Re}(m) = 1.2$ and effective size parameters in the range $x_{\mathrm{eff}} \in [2, 20]$ and for nearly normal incidence, $S_{11}^1(\mu_0, \mu_0, \pi)$ is small because $F_{11}(\pi)$ is small (Fig. 5), whereas the multiple-scattering contribution is large. As a result, the deviation of the copolarized enhancement factor from the value 2 is small (Plate 6, upper left diagram). In contrast, the (much) larger values of the backscattering phase function for nonabsorbing particles with larger refractive indices (Fig. 5) cause co-polarized enhancement factors significantly smaller than 2 (Plate 6, leftmost diagrams). The multiple-scattering contribution to the Stokes reflection matrix decreases with increasing angle of incidence, thus causing $\zeta_{vv}(\mu_0)$ to be a monotonically increasing function of μ_0 in most cases. Increased absorption also decreases the multiple-scattering contribution and, therefore, can strongly reduce $\zeta_{vv}(\mu_0)$ [Plate 6, diagrams for $\mathrm{Im}(m) = 0$, 0.002, and 0.01]. However, another effect of increasing the imaginary part of the refractive index is to significantly decrease the backscattering phase function (Fig. 5) and, thus, the first-order-scattering contribution [Eq. (43)]. Plate 6 shows that an interesting combined result of the two effects of increasing absorption can be an increase of the copolarized enhancement factor as $\mathrm{Im}(m)$ increases from 0.01 to 0.3.

Plate 7 shows that the cross-polarized enhancement factor $\zeta_{hv}(\mu_0)$ always increases with decreasing multiple-scattering contribution, i.e., with increasing absorption and/or decreasing μ_0, and can reach values very close to 2. In contrast, the opposite-circular enhancement factor can either decrease or increase with increasing $\mathrm{Im}(m)$ (Plate 8). It should be noted that accurate numerical computations of the cross-polarized enhancement factor $\zeta_{hv}(\mu_0)$ become difficult for strongly absorbing particles and/or for grazing illumination directions since both the nominator and the denominator in the right-hand side of Eq. (74) do not have a first-order-scattering component and become very small with vanishing multiple-scattering contribution. Therefore, such computations require the use of at least double-precision floating point variables. The ripple in contour lines seen in rightmost diagrams of Plate 7 may indicate that even the accuracy of double-precision variables is not quite sufficient for highly absorbing particles with $\mathrm{Im}(m) = 0.3$. In such cases the general inequality of Eq. (81) becomes an important check of numerical accuracy. Interestingly, although the general inequalities of Eqs. (81) and (82) do not rule out values of $\zeta_{hv}(\mu_0)$ and $\zeta_{oc}(\mu_0)$ less than unity, our practical computations suggest that 1 may be a more rigorous lower boundary for the cross-polarized and opposite-circular enhancement factors. Unfortunately, we have not been able to prove this analytically.

5. SUMMARY AND CONCLUSIONS

As was mentioned in the Introduction, Eqs. (11)–(15) represent one of very few rigorous results of the vector theory of coherent backscattering by sparsely distributed, independently scattering particles. In conjunction with accurate numerical solutions of the vector radiative transfer equation, they are essentially the only source of benchmark theoretical results for particles of any size, shape, and refractive index and can be used in analyzing results of controlled laboratory measurements and for checking the validity of approximate theoretical methods, first of all the diffusion approximation. For example, the accuracy of the values $\zeta_{vv}(1) = 1.88$, $\zeta_{hv}(1) = 1.17$, and $\mu_L^{\mathrm{diff}}(1) = 0.42$ obtained by Stephen and Cwilich[55] for the case of conservative ($w = 1$) Rayleigh

scattering using the diffusion approximation can be checked versus the accurate numbers $\zeta_{vv}(1) = 1.7521$, $\zeta_{hv}(1) = 1.1201$, and $\mu_L^{diff}(1) = 0.5167$ obtained in Ref. 39.

In this paper, we have used Eqs. (10)–(15) along with numerically accurate solutions of the vector radiative transfer equation to perform a theoretical survey of diffuse and coherent backscattering for a wide range of particle size parameters and real and imaginary parts of the refractive index and discussed the effect of these parameters on the photometric and polarization characteristics of the radar return. The results of this survey are summarized in Sec. 4. Not surprisingly, we have found that in many cases the polarimetric characteristics of the radar return are complex functions of the scattering medium parameters. This complexity results from the complexity of the process of multiple scattering of polarized radiation and necessitates the use of elaborated techniques, like the one employed in this study, in theoretical computations.

Equations (64), (65), (68), and (69) show that the linear and circular polarization ratios (both diffuse and full) for a discrete random medium composed of spherical particles would be equal to zero in the absence of multiple scattering. Therefore, it is multiple scattering that produces nonzero polarization ratios for a medium composed of spherical scatterers. It is important to emphasize that multiple scattering can strongly depolarize even the diffuse background (Plates 2 and 3); therefore, it is not true that the only cause of depolarization is coherent backscattering—the statement that can be found in some applied papers. What coherent backscattering can do is to significantly change the polarization ratios of the diffuse background: increase the circular polarization ratio and either increase or decrease the linear polarization ratio. Although the aim of this paper is not to apply the theory to analyze some real measurements, our computations demonstrate that the multiple scattering mechanism can indeed be relevant to radar observations of snow- and ice-covered planetary surfaces (cf. Ref. 17).

It is important to note that multiple scattering in optically thick media is not the only mechanism producing nonzero backscattering polarization ratios. Another mechanism which can work even in the absence of multiple scattering is single scattering by nonspherical particles. That mechanism was studied in Ref. 46 for randomly oriented nonspherical particles and in Refs. 61 and 62 for fully and partially aligned nonspherical particles. Interestingly, despite the different nature of depolarization, the inequalities of Eqs. (83), (92), and (93) also apply to single scattering by randomly oriented nonspherical particles provided that the particles have a plane of symmetry and/or particles and their mirror counterparts occur in equal numbers.[46] Therefore, it may be difficult in practice to conclude which of the two mechanisms is primarily responsible for observed depolarization.

For simplicity, we have ignored in this study the effect of spatial correlations of densely packed particles and the fact that in densely packed media scattering particles can be in the near-field zone of each other, thus questioning the applicability of Mie theory to computing their single-scattering properties. As we have already mentioned, calculations of Ref. 38 suggest that the primary effect of spatial correlations may be to modify the particles' forward-scattering behavior, thus indicating that backscattering radiative transfer calculations can be reasonably accurate even for densely packed particles. Also, the results of Ref. 56 may indicate that the near-field effects are not necessarily appreciable, especially if the distance between the centers of wavelength-sized particles is greater than two times their diameter. One way to take into account the near-field effects is to include additional, range-dependent terms in the transverse scattered fields in computing the Mueller scattering matrix and to use this modified Mueller matrix in the radiative transfer equation.[57] Another way of dealing with this problem is to solve Maxwell's equations directly for a configuration consisting of a very large number of densely packed scatterers by using the T-matrix approach[58,59] or the discrete dipole approximation.[60] Although the second approach can be more accurate, it is much more complicated and computer intensive. In any case, future investigations should demonstrate whether or not the near-field effects can change the photometric and polarization characteristics of coherent backscattering significantly.

In this first paper of a series, we have only considered optically semi-infinite media composed of spherical particles. Furthermore, we did not consider the practically important case of unpolarized incident radiation relevant to passive planetary observations in the visible and near infrared spectral regions. In a forthcoming paper, we plan to examine the effects of finite optical

thickness and particle nonsphericity, and also to study reflectance characteristics of a particulate medium illuminated by unpolarized light.

Acknowledgements—I thank J. W. Hovenier for his comments and N. T. Zakharova for help with graphics. This work was supported in part by the NASA Goddard Institute for Space Studies Planetary Research Program and by the NASA Earth Observing System Project in providing for the Earth Observing Scanning Polarimeter instrument and analysis algorithm development.

REFERENCES

1. *Scattering in Volumes and Surfaces*, M. Nieto-Vesperinas and J. C. Dainty, eds., North-Holland, Amsterdam (1990).
2. *Scattering and Localization of Classical Waves in Random Media*, P. Sheng, ed., World Scientific, Singapore (1990).
3. Yu. N. Barabanenkov, Yu. A. Kravtsov, V. D. Ozrin, and A. I. Saichev, in *Progress in Optics XXIX*, E. Wolf, ed., p. 65, Elsevier, New York, NY (1991).
4. M. I. Mishchenko, *Mon. Not. R. Astron. Soc.* **254,** 15P (1992).
5. M. I. Mishchenko and J. M. Dlugach, *Planet. Space Sci.* **41,** 173 (1993).
6. M. I. Mishchenko, *Astrophys. J.* **411,** 351 (1993).
7. Yu. G. Shkuratov, *Kinem. Fiz. Nebes. Tel* **4,** 33 (1988); *Astron. Vestnik* **25,** 152 (1991).
8. K. Muinonen, in *Proc. URSI Electromagn. Theory Symp.* (Stockholm), p. 428; Ph.D. thesis, Univ. Helsinki (1990).
9. B. Hapke, *Icarus* **88,** 407 (1990).
10. B. W. Hapke, R. M. Nelson, and W. D. Smythe, *Science* **260,** 509 (1993).
11. K. Muinonen, in *Asteroids, Comets, Meteors 1993*, A. Milani et al, eds., p. 271, Kluwer, Dordrecht (1994).
12. M. I. Mishchenko, *Earth Moon Planets* **58,** 127 (1992).
13. K. J. Peters, *Phys. Rev. B* **46,** 801 (1992).
14. S. J. Ostro, D. B. Campbell, R. A. Simpson, R. S. Hudson, J. F. Chandler, K. D. Rosema, I. I. Shapiro, E. M. Standish, R. Winkler, D. K. Yeomans, R. Velez, and R. M. Goldstein, *J. Geophys. Res.* **97,** 18,227 (1992).
15. B. A. Campbell, R. E. Arvidson, and M. K. Shepard, *J. Geophys. Res.* **98,** 17,099 (1993).
16. B. J. Butler, D. O. Muhleman, and M. A. Slade, *J. Geophys. Res.* **98,** 15,003 (1993).
17. S. J. Ostro, *Rev. Mod. Phys.* **65,** 1235 (1993).
18. L. Tsang, J. A. Kong, and R. T. Shin, *Theory of Microwave Remote Sensing*, Wiley, New York, NY (1985).
19. M. B. van der Mark, M. P. van Albada, and A. Lagendijk, *Phys. Rev. B* **37,** 3575 (1988).
20. E. Akkermans, P. E. Wolf, R. Maynard, and G. Maret, *J. Phys. (Paris)* **49,** 77 (1988).
21. M. P. van Albada, M. B. van der Mark, and A. Lagendijk, *J. Phys. D* **21,** S28 (1988).
22. M. P. van Albada and A. Lagendijk, *Phys. Rev. B* **36,** 2353 (1987).
23. F. C. MacKintosh and S. John, *Phys. Rev. B* **37,** 1884 (1988).
24. M. I. Mishchenko, *JOSA A* **9,** 978 (1992).
25. V. D. Ozrin, *Waves Random Media* **2,** 141 (1992).
26. D. S. Saxon, *Phys. Rev.* **100,** 1771 (1955).
27. A. P. Prishivalko, V. A. Babenko, and V. N. Kuz'min, *Scattering and Absorption of Light by Inhomogeneous and Anisotropic Spherical Particles*, Nauka i Tekhnika, Minsk (1984) (in Russian).
28. A. Ishimaru and L. Tsang, *JOSA A* **5,** 228 (1988).
29. S. Chandrasekhar, *Radiative Transfer*, Clarendon, London (1950).
30. A. Ishimaru and C. W. Yeh, *JOSA A* **1,** 359 (1984).
31. J. E. Hansen and L. D. Travis, *Space Sci. Rev.* **16,** 527 (1974).
32. W. A. de Rooij, Ph.D. thesis, Free University, Amsterdam (1985).
33. R. D. M. Garcia and C. E. Siewert, *JQSRT* **36,** 401 (1986).
34. J. W. Hovenier, *Astron. Astrophys.* **13,** 7 (1971); J. F. de Haan, P. W. Bosma, and J. W. Hovenier, *Astron. Astrophys.* **183,** 371 (1987).
35. R. D. M. Garcia and C. E. Siewert, *JQSRT* **41,** 117 (1989).
36. M. I. Mishchenko, *JQSRT* **43,** 163 (1990).
37. M. I. Mishchenko, *Opt. Lett.* **21,** 623 (1996).
38. M. I. Mishchenko, *JQSRT* **52,** 95 (1994).
39. M. I. Mishchenko, *Phys. Rev. B* **44,** 12,597 (1991).
40. P. E. Wolf, G. Maret, E. Ackermans, and R. Maynard, *J. Phys. (Paris)* **49,** 63 (1988).
41. J. J. van Zyl and F. T. Ulaby, in *Radar Polarimetry for Geoscience Applications*, F. T. Ulaby and C. Elachi, eds., p. 17, Artech House, Norwood, MA (1990).
42. S. R. Cloude and E. Pottier, *Opt. Engng* **34,** 1599 (1995); *IEEE Trans. Geosci. Remote Sens.* **34,** 498 (1996).
43. J. W. Hovenier and C. V. M. van der Mee, *Astron. Astrophys.* **128,** 1 (1983).
44. V. A. Ambartsumian, *Astron. Zh. (Sov.)* **19,** 30 (1942).
45. H. C. van de Hulst, *Light Scattering by Small Particles*, Wiley, New York, NY (1957).

46. M. I. Mishchenko and J. W. Hovenier, *Opt. Lett.* **20,** 1356 (1995).
47. H. C. van de Hulst, *Multiple Light Scattering*, Academic Press, New York, NY (1980).
48. W. A. de Rooij and C. C. A. H. van der Stap, *Astron. Astrophys.* **131,** 237 (1984).
49. W. A. de Rooij and H. Domke, *JQSRT* **31,** 285 (1984).
50. J. M. Dlugach and E. G. Yanovitskij, *Icarus* **22,** 66 (1974).
51. J. E. Hansen, *J. Atmos. Sci.* **28,** 1400 (1971).
52. F. T. Ulaby, R. K. Moore, and A. K. Fung, *Microwave Remote Sensing*, Addison–Wesley, Reading, MA (1981).
53. J. W. Hovenier, H. C. van de Hulst, and C. V. M. van der Mee, *Astron. Astrophys.* **157,** 301 (1986).
54. P. den Outer, Ph.D. thesis, Amsterdam Univ. (1995).
55. M. J. Stephen and G. Cwilich, *Phys. Rev. B* **34,** 7564 (1986).
56. M. I. Mishchenko, D. W. Mackowski, and L. D. Travis, *Appl. Opt.* **34,** 4589 (1995).
57. A. K. Fung and H. J. Eom, *IEEE Trans. Geosci. Remote Sens.* **23,** 761 (1985).
58. Y. C. Tzeng and A. K. Fung, *J. Electromagn. Waves Appl.* **8,** 61 (1994).
59. D. W. Mackowski and M. I. Mishchenko, *JOSA A* **13,** in press (1996).
60. K. Lumme and J. Rahola, *Astrophys. J.* **425,** 653 (1994).
61. E. Rignot, *J. Geophys. Res.* **100,** 9389 (1995).
62. C. Tang and K. Aydin, *IEEE Trans. Geosci. Remote Sens.* **33,** 93 (1995).